European Journal of Mechanics A/Solids 42 (2013) 358–375

Contents lists available at ScienceDirect

European Journal of Mechanics A/Solids

journal homepage: www.elsevier.com/locate/ejmsol

Approximate modelling of resulting dry friction forces and rolling resistance for elliptic contact shape

Grzegorz Kudra*, Jan Awrejcewicz

Lodz University of Technology, Department of Automation and Biomechanics (K-16), 1/15 Stefanowskiego St., 90-924 Łódź, Poland

ARTICLE INFO

Article history:
Received 25 January 2013
Accepted 10 July 2013
Available online 23 July 2013

Keywords:
Friction modelling
Rolling resistance
Contour friction

ABSTRACT

There are many examples of mechanical systems with non-point friction contacts (billiard ball, Thompson top, wobblestone, electric polishing machine, the wobblestone, the Celtic stone), where the assumption of one-dimensional dry friction model do not necessarily lead to satisfactory accuracy of the numerical simulation. Moreover the rolling resistance often plays an important role in such systems. The paper is devoted to the problem of developing an approximate coupled model of resulting dry friction force and moment as well as rolling resistance, suitable for fast numerical simulation of rigid bodies with friction contacts, i.e. allowing to avoid the space discretization. An integral model of dry friction components is built under assumption of classical Coulomb friction law and fully developed sliding on the contact area of general shape and arbitrary contact pressure distribution. Then the special model of stress distribution over the elliptic contact area is developed, being a kind of generalization of Hertzian normal stress distribution, with addition of special distortion related to the rolling resistance. Finally some original approximate models of friction force and moment are proposed, based on Padé approximants and their generalizations as well as in the form of piecewise polynomial functions.

1. Introduction

If the contact between two bodies is very small (the point contact), the sliding friction force opposes the sliding relative velocity and can be successfully modelled by the use of classical one-dimensional Coulomb friction law. In this case the friction torque (drilling friction) and its influence on sliding friction force can be neglected (since the contact point cannot transmit a torque). But there are many cases of dynamical behaviour of mechanical systems (billiard ball, Thompson top, wobblestone, electric polishing machine) which cannot be mathematically modelled (in order to obtain correct numerical simulation) or explained by the use of the assumption of one-dimensional dry friction model. One can find in the literature some attempts to develop approximate models of friction forces for finite contact area, which would be suitable for fast numerical simulation of rigid bodies, i.e. allowing to avoid the space discretization around the contact area.

Contensou (1962) noticed that relative normal angular velocity (spin) is important for the dynamics of some mechanical systems where the contact between two bodies or spin is relatively large. Assuming fully developed sliding and Coulomb friction law valid on some circular contact area, he presented friction force as a function of two variables: relative sliding velocity of the centre of the contact between two interacting bodies and relative normal angular velocity. He presented the results in integral and numerical forms for the contact stress distribution according to Hertz theory. Then the results of Contensou were essentially developed by Zhuravlev (1998, 2003) by giving exact analytical expressions for friction force and torque as well as corresponding linear Padé approximations more convenient to use in practical problems of modelling and simulation. We will refer to the coupled model of friction force and torque as Coulomb–Contensou friction model. This direction of research led subsequently to the second-order Padé approximants (Kireenkov, 2008), more accurate and suitable for qualitative analysis. Using the same methodology, the problem of friction modelling in the case of axial symmetry of the contact stress distribution over the contact area is approached (Kireenkov, 2005) (the elliptic contact patch with Hertzian stress distribution is such a case). The integral forms of coefficients of the corresponding Padé approximants were given, however, without any concrete, even numerical example. A three-dimensional friction model for circular areas but with the coupling between friction and rolling resistance, where rolling resistance is a result of distortion of contact stress distribution is developed in the work (Kireenkov, 2008). It can be noticed that the proposed model of rolling resistance is compatible and logically coherent with the mechanism of rolling friction caused by

* Corresponding author. Tel.: +48 426312339.
E-mail address: grzegorz.kudra@p.lodz.pl (G. Kudra).

0997-7538/$ – see front matter © 2013 Elsevier Masson SAS. All rights reserved.
http://dx.doi.org/10.1016/j.euromechsol.2013.07.005

elastic hysteresis losses (the main component of rolling resistance in many real systems) (Greenwood et al., 1961; Johnson, 1985).

There exist other approaches to the above described problem. In the work (Leine and Glocker, 2003) the coupled friction model for circular contact area with fully developed sliding and central symmetry of contact stress distribution (without rolling resistance) was approximated by the use of Taylor expansion of the velocity pseudo potential and then used in the Thompson top modelling and simulation. The piecewise linear approximation of the three-dimensional friction model for elliptic contact area and the Hertz stress distribution (without rolling resistance) was presented in paper (Kosenko and Aleksandrov, 2009) which showed that the proposed model was more accurate than the linear Padé approximants.

As mentioned above, there were some approaches to model rolling resistance along with the friction modelling. However, a question of the nature of rolling friction arises. Classically, it is understood as a resistance against relative angular velocity of the contacting bodies tangential to the plane of contact. But this model often leads to cumbersome and questionable results. Some authors use the concept of contour friction as resistance against the movement of contact point along the body (Leine, 2009; Leine et al., 2005; Leine and Van De Wouw, 2008). These two models give the same results in some special cases (for example when there is no slip between contacting bodies), but in general they differ essentially. However, the proposed models of contour friction do not take into account the shape of the contact patch. Moreover, coupling with the contact stress distribution and components of the dry friction model is also neglected.

In the present work, based on some extensions of Padé approximants, we propose an approximate coupled model of dry friction components (spatial force and torque) and rolling resistance for the contact with fully developed sliding and Coulomb friction law assumed. The paper is organized as follows. In Sect. 2 the integral model of friction force and torque for general shape of plane contact is introduced and some expressions useful in developing of different approximate models are given. Sect. 3 limits the considerations to the elliptic shape of contact, where the model of normal stress distribution and integrals from expressions is given. The solutions to certain integrals occurring in the general integral model of friction are given. In Sect. 4 we develop and present approximate friction models. Sect. 5 gives some final remarks.

2. Integral model of sliding friction force and torque for general shape of plane contact

Let us consider two bodies 1 and 2 (Fig. 1) in contact on a certain area F of general shape. In what follows, we assume the following properties of the contact:

1. The contact F is locally plane.
2. On every element dF of the contact F, the classic Coulomb friction laws are valid, and the friction coefficient does not depend on local relative velocity.
3. The friction coefficient is constant on whole contact area F.
4. The sliding on the contact area F is fully developed.
5. The strains of the bodies do not influent on local relative velocities in the contact plane.

The assumptions 1, 4 and 5 mean that the relative motion of the bodies in the contact plane can be treated as locally plane motion of rigid body.

Although the bodies in their global dynamics can be assumed as rigid (i.e. the deformations are negligible) and the contact between them can be non-conforming, the shape and size of small contact area F can play a considerable role in the friction model. Point A is the nominal point of contact. In the case of non-conforming contact, this is a point at which two bodies touch, brought into contact by negligibly small force. In the case of conforming (but plane) contact this is a certain arbitrarily chosen point in the contact plane. We introduce the coordinate system $Axyz$, where axes x and y lie in the contact plane and z axis coincides with the common normal to the two surfaces at A. The directions of axes x and y are chosen for convenience to coincide with certain characteristic directions of the body or contact area profiles.

The motion of body 1 (taken as a rigid body) is defined by the linear velocity $\mathbf{v}_1$ of point A_1 (the body-fixed point instantly coinciding with the point of contact A) and angular velocity $\boldsymbol{\omega}_1$. Likewise, we define the motion of body 2 by velocities $\mathbf{v}_2$ (the velocity of point A_2) and $\boldsymbol{\omega}_2$. We can now define *sliding* (Johnson, 1985) as the relative linear velocity between the two bodies at point A and denote it by $\mathbf{v}_s$

$$\mathbf{v}_s = \mathbf{v}_2 - \mathbf{v}_1. \tag{1}$$

The component of $\mathbf{v}_s$ along the axis z is equal to zero ($v_{sz} = 0$) since we assume here the continuous contact, i.e. the surfaces of the bodies are neither separating nor overlapping.

Similarly, we define the relative angular velocity between the two bodies and denote it by $\boldsymbol{\Delta\omega}$

$$\boldsymbol{\Delta\omega} = \boldsymbol{\omega}_2 - \boldsymbol{\omega}_1. \tag{2}$$

The above vector can be decomposed into two perpendicular components in the following way

$$\boldsymbol{\Delta\omega} = \underbrace{\Delta\omega_x \mathbf{e}_x + \Delta\omega_y \mathbf{e}_y}_{\boldsymbol{\omega}_r = \omega_{rx}\mathbf{e}_x + \omega_{ry}\mathbf{e}_y} + \underbrace{\Delta\omega_z \mathbf{e}_z}_{\boldsymbol{\omega}_s = \omega_s \mathbf{e}_z} = \boldsymbol{\omega}_r + \boldsymbol{\omega}_s, \tag{3}$$

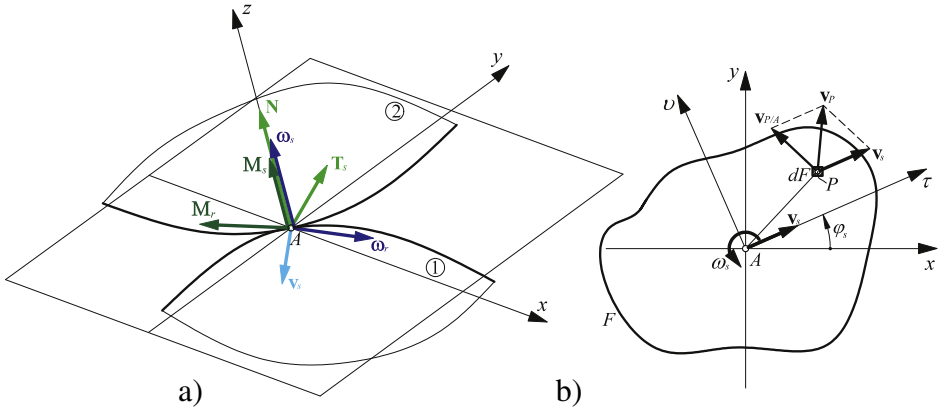

Fig. 1. Two bodies in contact: contact forces and relative velocities (a) and general case of plane contact area (b).

where $\mathbf{e}_x$, $\mathbf{e}_y$ and $\mathbf{e}_z$ are the unit vectors of the corresponding axes, while $\boldsymbol{\omega}_r$ and $\boldsymbol{\omega}_s$ are the angular velocities of *rolling* and *spin* motion, respectively (Johnson, 1985). Now, any relative motion of contacting surfaces can be regarded as a combination of sliding, rolling and spin (see vectors $\mathbf{v}_s$, $\boldsymbol{\omega}_r$ and $\boldsymbol{\omega}_s$, respectively exhibited in Fig. 1a).

Fig. 1a shows also forces and torques acting on body 2 at point A. Resultant force $\mathbf{R}$ transmitted from one surface to another through the point of contact is decomposed into normal force $\mathbf{N}$ and tangential force $\mathbf{T}_s$ sustained by friction. Likewise, the resultant torque transmitted by the contact is decomposed into *rolling resistance* $\mathbf{M}_r$ (lying in the tangent plane) and *spin moment* $\mathbf{M}_s$ (along the common normal to the two surfaces at A) arising from friction within the contact area.

Very often, rolling velocity $\boldsymbol{\omega}_r$ is used as a basic kinematic quantity in the process of modelling of rolling resistance $\mathbf{M}_r$ understood in a classical way, i.e. as resistance against rolling angular velocity. However, this approach is sometimes replaced by the concept of *contour friction* as certain resistance opposing the *contour velocity* understood as the relative motion of contact point A with respect to the body (cf. Leine, 2009; Leine et al., 2005; Leine and Van De Wouw, 2008 and Sect. 3.1). Each body has its own contour velocity for which the contour friction can be defined. Assuming that the frame of reference $Axyz$ moves at linear velocity $\mathbf{v}_A$ of its origin and rotates at angular velocity $\boldsymbol{\omega}_A$, we can now define (for the further purposes of the work) contour velocities $\mathbf{v}_{r1}$ and $\mathbf{v}_{r2}$ (for body 1 and 2, respectively) in the following way

$$\mathbf{v}_{r1} = \mathbf{v}_A - \mathbf{v}_1, \quad \mathbf{v}_{r2} = \mathbf{v}_A - \mathbf{v}_2. \tag{4}$$

In order to develop a dimensionless model of friction for the contact area presented in Fig. 1b, we now assume that all quantities defined above refer to the dimensionless length related to some characteristic real dimension $\widehat{a}$ of the contact area, therefore dimensionless coordinates of the element $\mathrm{d}F$ (point P) position are $x = \widehat{x}/\widehat{a}$ and $y = \widehat{y}/\widehat{a}$, where $\widehat{x}$ and $\widehat{y}$ are the corresponding real coordinates, whereas dimensionless element of the area equals $\mathrm{d}F = \mathrm{d}\widehat{F}/\widehat{a}^2$, where $\mathrm{d}\widehat{F}$ is the real element. A consequence of dimensionless length is the relation $\mathbf{v}_s = \widehat{\mathbf{v}}_s/(\alpha\widehat{a})$, where $\widehat{\mathbf{v}}_s$ is the real sliding velocity of point A and α is the additional parameter defining the used time $t = \alpha\widehat{t}$, where $\widehat{t}$ is the real time. Then, spin velocity reads $\boldsymbol{\omega}_s = \widehat{\boldsymbol{\omega}}_s/\alpha$, where $\widehat{\boldsymbol{\omega}}_s$ is the real spin velocity of the contact. In addition, coordinate system $A\tau v$ lying in the contact plane is introduced, where τ axis has the direction of velocity $\mathbf{v}_s$ specified by angle φ_s.

Assuming that the classical Coulomb friction law is valid on each element $\mathrm{d}F$ at relative velocity $\mathbf{v}_P = \widehat{\mathbf{v}}_P/(\alpha\widehat{a})$ (where $\widehat{\mathbf{v}}_P$ is its real counterpart), we obtain the following dimensionless form of the infinitesimal sliding (dry) friction force $\mathrm{d}\mathbf{T}_s = \mathrm{d}\widehat{\mathbf{T}}_s/(\mu\widehat{N})$ (where $\mathrm{d}\widehat{\mathbf{T}}_s$ is the corresponding real force, $\widehat{N}$ is the normal component of resultant real force of interaction between bodies and μ is the dry friction coefficient), acting on the body lying above area F, and the corresponding dimensionless infinitesimal moment of friction force $\mathrm{d}\mathbf{M}_s = \mathrm{d}\widehat{\mathbf{M}}_s/(\widehat{a}\mu\widehat{N})$ (where $\mathrm{d}\widehat{\mathbf{M}}_s$ is its real counterpart) with respect to pole A

$$\begin{aligned} \mathrm{d}\mathbf{T}_s &= -\sigma(x,y)\frac{\mathbf{v}_P}{\|\mathbf{v}_P\|}\mathrm{d}F, \\ \mathrm{d}\mathbf{M}_s &= \boldsymbol{\rho}\times\mathrm{d}\mathbf{T}_s. \end{aligned} \tag{5}$$

In Eq. (5), the dimensionless normal stress distribution $\sigma(x,y) = \widehat{\sigma}(x,y)\widehat{a}^2/\widehat{N}$ has been introduced (where $\widehat{\sigma}(x,y)$ is the real stress distribution), whereas $\boldsymbol{\rho} = \widehat{\boldsymbol{\rho}}/\widehat{a} = \overrightarrow{AP}$ is the dimensionless vector coupling pole A with element $\mathrm{d}F$ (where $\widehat{\boldsymbol{\rho}}$ is its real counterpart). One can find easily that the non-dimensional relation is equivalent to the dimensional differential form of the Coulomb friction law for element $\mathrm{d}\widehat{F}$: $\mathrm{d}\widehat{T}_s = -\mu\widehat{\sigma}(x,y)\mathrm{d}\widehat{F}\widehat{\mathbf{v}}_P/\|\widehat{\mathbf{v}}_P\|$ and $\mathrm{d}\widehat{\mathbf{M}}_s = \widehat{\boldsymbol{\rho}}\times\mathrm{d}\widehat{\mathbf{T}}_s$. Note, that relations (5) and all further formulae and models presented in this section do not depend on parameter α.

The resultant dimensionless friction force and dimensionless friction torque are as follows

$$\begin{aligned} \mathbf{T}_s &= -\iint_F \sigma(x,y)\frac{\mathbf{v}_P}{\|\mathbf{v}_P\|}\mathrm{d}F, \\ \mathbf{M}_s &= -\iint_F \sigma(x,y)\frac{\boldsymbol{\rho}\times\mathbf{v}_P}{\|\mathbf{v}_P\|}\mathrm{d}F. \end{aligned} \tag{6}$$

Taking into consideration that $\mathbf{v}_P = \mathbf{v}_s + \boldsymbol{\omega}_s\times\boldsymbol{\rho}$ (where $\boldsymbol{\omega}_s\times\boldsymbol{\rho} = \mathbf{v}_{P/A}$, $\mathbf{v}_s = v_s\cos\varphi_s\mathbf{e}_x + v_s\sin\varphi_s\mathbf{e}_y$, $\boldsymbol{\omega}_s = \omega_s\mathbf{e}_z$ and $\boldsymbol{\rho} = x\mathbf{e}_x + y\mathbf{e}_y$) we obtain the following relations

$$\begin{aligned} &\mathbf{v}_P = v_{Px}\mathbf{e}_x + v_{Py}\mathbf{e}_y = (v_s\cos\varphi_s - \omega_s y)\mathbf{e}_x + (v_s\sin\varphi_s + \omega_s x)\mathbf{e}_y, \\ &\boldsymbol{\rho}\times\mathbf{v}_P = \left(xv_{Py} - yv_{Px}\right)\mathbf{e}_z = \left(\omega_s\left(x^2+y^2\right) + v_s x\sin\varphi_s - v_s y\cos\varphi_s\right)\mathbf{e}_z. \end{aligned} \tag{7}$$

By the use of v_s and ω_s we have denoted the projections of vectors $\mathbf{v}_s$ and $\boldsymbol{\omega}_s$ onto axes τ and z correspondingly, i.e. $v_s = v_{s\tau}$ and $\omega_s = \omega_{sz}$. Since the direction of axis τ is determined by the angle $0 \le \varphi_s < 2\pi$, without loss of generality, one can assume that $v_s = \|\mathbf{v}_s\| \ge 0$. On the other hand, assuming generalization of v_s, taking any real value can be convenient in some cases. Then angle φ_s, defining the direction of the τ axis, can be limited to the half of full rotation (e.g. $0 \le \varphi_s < \pi$).

From Eq. (6) and taking into account (7), we get the following integral form of dry friction model in the $Axyz$ coordinate system

$$\begin{aligned} T_{sx}(v_s,\omega_s,\varphi_s) &= \iint_F \sigma(x,y)\frac{v_s\cos\varphi_s - \omega_s y}{\sqrt{(v_s\cos\varphi_s - \omega_s y)^2 + (v_s\sin\varphi_s + \omega_s x)^2}}\mathrm{d}x\mathrm{d}y, \\ T_{sy}(v_s,\omega_s,\varphi_s) &= \iint_F \sigma(x,y)\frac{v_s\sin\varphi_s + \omega_s x}{\sqrt{(v_s\cos\varphi_s - \omega_s y)^2 + (v_s\sin\varphi_s + \omega_s x)^2}}\mathrm{d}x\mathrm{d}y, \\ M_s(v_s,\omega_s,\varphi_s) &= \iint_F \sigma(x,y)\frac{\omega_s\left(x^2+y^2\right) + v_s x\sin\varphi_s - v_s y\cos\varphi_s}{\sqrt{(v_s\cos\varphi_s - \omega_s y)^2 + (v_s\sin\varphi_s + \omega_s x)^2}}\mathrm{d}x\mathrm{d}y, \end{aligned} \tag{8}$$

where the signs were changed in order to simplify the notation. It means that the friction force and torque are $\mathbf{T}_s = -T_{sx}\mathbf{e}_x - T_{sy}\mathbf{e}_y$ and $\mathbf{M}_s = -M_s\mathbf{e}_z$, respectively.

Assuming the following relations

$$v_s = \lambda_s\cos\theta_s, \quad \omega_s = \lambda_s\sin\theta_s, \quad \text{where } \lambda_s = \sqrt{v_s^2 + \omega_s^2} \tag{9}$$

(geometrical interpretation of φ_s and $-\pi/2 \le \theta_s \le \pi/2$ variables is presented in Fig. 2), one can reduce the number of arguments of the functions (8), obtaining the following form of the model

$$\begin{aligned} T_{sx}(\varphi_s,\theta_s) &= \iint_F \frac{\sigma(x,y)[\cos\theta_s\cos\varphi_s - y\sin\theta_s]}{\sqrt{(\cos\theta_s\cos\varphi_s - y\sin\theta_s)^2 + (\cos\theta_s\sin\varphi_s + x\sin\theta_s)^2}}\mathrm{d}x\mathrm{d}y, \\ T_{sy}(\varphi_s,\theta_s) &= \iint_F \frac{\sigma(x,y)[\cos\theta_s\sin\varphi_s + x\sin\theta_s]}{\sqrt{(\cos\theta_s\cos\varphi_s - y\sin\theta_s)^2 + (\cos\theta_s\sin\varphi_s + x\sin\theta_s)^2}}\mathrm{d}x\mathrm{d}y, \\ M_s(\varphi_s,\theta_s) &= \iint_F \sigma(x,y)\frac{\sin\theta_s\left(x^2+y^2\right) + x\cos\theta_s\sin\varphi_s - y\cos\theta_s\cos\varphi_s}{\sqrt{(\cos\theta_s\cos\varphi_s - y\sin\theta_s)^2 + (\cos\theta_s\sin\varphi_s + x\sin\theta_s)^2}}\mathrm{d}x\mathrm{d}y. \end{aligned} \tag{10}$$

The exact integral forms ((8) and (10)) of the friction model are inconvenient to use directly in mathematical modelling and numerical simulations for most typical special cases of shape of the contact area and normal stress distribution. One of the difficulties is time consuming numerical integration over contact area F during the simulation process. An additional difficulty in numerical integration process is the existence of singularities of the functions ((8) and (10)) in the instant rotation centre. On the other hand, for some

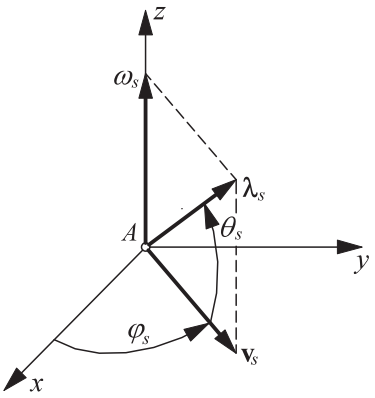

Fig. 2. Geometrical interpretation of φ_s and θ_s variables.

cases, e.g. for circular contact region, it is possible to find an analytical solution to Eq. (8) (Kireenkov, 2005; Leine and Glocker, 2003; Zhuravlev, 1998). But the mathematical model obtained in this way is relatively complex and inconvenient in direct use. The solution to the problem can be some kind of approximation of the exact integral model.

On this level of generality one can find some universal relations for the plane region of contact, concerning values and partial derivatives of functions (8) for $v_s = 0$ (assuming $\omega_s \neq 0$) and for $\omega_s = 0$ (assuming $v_s \neq 0$), which can be useful in developing some kinds of approximating models. The corresponding values of functions (8) are as follows

$$\begin{aligned} T_{sx}|_{v_s=0} &= -c^{(x,y)}_{0,1,1}\tfrac{\omega_s}{|\omega_s|}, \quad T_{sx}|_{\omega_s=0} = c^{(x,y)}_{0,0,0}c_\varphi\tfrac{v_s}{|v_s|}, \\ T_{sy}|_{v_s=0} &= c^{(x,y)}_{1,0,1}\tfrac{\omega_s}{|\omega_s|}, \quad T_{sy}|_{\omega_s=0} = c^{(x,y)}_{0,0,0}s_\varphi\tfrac{v_s}{|v_s|}, \\ M_s|_{v_s=0} &= c^{(x,y)}_{0,0,-1}\tfrac{\omega_s}{|\omega_s|}, \quad M_s|_{\omega_s=0} = \left(c^{(x,y)}_{1,0,0}s_\varphi - c^{(x,y)}_{0,1,0}c_\varphi\right)\tfrac{v_s}{|v_s|}, \end{aligned} \tag{11}$$

where for brevity the following notation has been used

$$s_\varphi = \sin\varphi_s, \quad c_\varphi = \cos\varphi_s, \tag{12}$$

$$c^{(\zeta,\eta)}_{i,j,k} = \iint_F \zeta^i\eta^j\left(\zeta^2+\eta^2\right)^{-\frac{k}{2}}\sigma(\zeta,\eta)\mathrm{d}\zeta\mathrm{d}\eta, \tag{13}$$

and where

$$c^{(\zeta,\eta)}_{0,0,0} = \iint_F \sigma(\zeta,\eta)\mathrm{d}\zeta\mathrm{d}\eta = 1, \tag{14}$$

(because of the non-dimensional form of the normal stress distribution $\sigma(x,y)$) and where (ζ,η) are the coordinates of an arbitrary rectangular coordinate system in the plane of the contact zone F. The analogous expressions for the first and second order partial derivatives of the functions (8) are given in Appendix A.

One can notice that the corresponding values and derivatives of functions (8) for $v_s = 0$ (assuming $\omega_s \neq 0$) and for $\omega_s = 0$ (assuming $v_s \neq 0$) for an arbitrary normal stress distribution depend only on integrals (13) which can be found for many special cases of contact area shape and normal stress distribution. Moreover, in the case of invariant contact pressure distribution, the integrals $c^{(\zeta,\eta)}_{i,j,k}$ are the constant parameters, and they can be identified from the experiment.

3. A coupled model of sliding and rolling friction for elliptic contact shape

3.1. A model of normal stress distribution coupled with rolling friction

We start from an assumption of certain non-dimensional normal stress $\sigma'_0(\rho')$ distribution over the non-dimensional circular zone $F'(\iint_{F'}\sigma'_0\mathrm{d}F' = 1)$ presented in Fig. 3a, depending only on distance $\rho' = \sqrt{x'^2+y'^2}$ from centre A of the area F', where x' and y' are the coordinates of a point of contact zone in the Cartesian coordinate system $Ax'y'$. Each quantity corresponding to the area F' and being the counterpart of a quantity X corresponding to the area F exhibited by Fig. 1, is denoted by X'.

Then, in order to generate the rolling resistance torque $\mathbf{M}'_r$, we assume that initial stress distribution $\sigma'_0(\rho')$ undergoes distortion along the axis τ'_r of the rectangular coordinate system $A\tau'_rv'_r$ and gets the following form

$$\sigma'(x',y') = \sigma'_0\left(\sqrt{x'^2+y'^2}\right)(1+d(x'\cos\gamma'+y'\sin\gamma')), \tag{15}$$

where γ' is the angle describing direction of the axis τ'_r, while $0 \leq d \leq 1$ (the upper limit results from the condition of non-negative normal stress values) is a certain non-dimensional rolling resistance coefficient related to the magnitude of the contact zone. In the above expression, $x'\cos\gamma'+y'\sin\gamma'$ is the distance of point (x',y') from the axis v'_r. The pressure distribution $\sigma'(x',y')$ has the centre at point S' lying on the axis τ'_r and generate the non-dimensional rolling resistance torque $\mathbf{M}'_r$ of magnitude $M'_r = AS' = \iint_F \sigma'(x',y')\tau'_r\mathrm{d}F' / \iint_F \sigma'(x',y')\mathrm{d}F' = \pi d\int_0^1 \sigma'_0(\rho')\rho'^3\mathrm{d}\rho'$ (the resultant normal reaction is equal to one).

Model (15) corresponds to the proposition of Kireenkov (2008) based on the work of Svedenius (2003), concerning modelling of the rolling resistance of motor-car wheels. However, they define direction τ'_r in such a way that the rolling resistance torque $\mathbf{M}'_r$

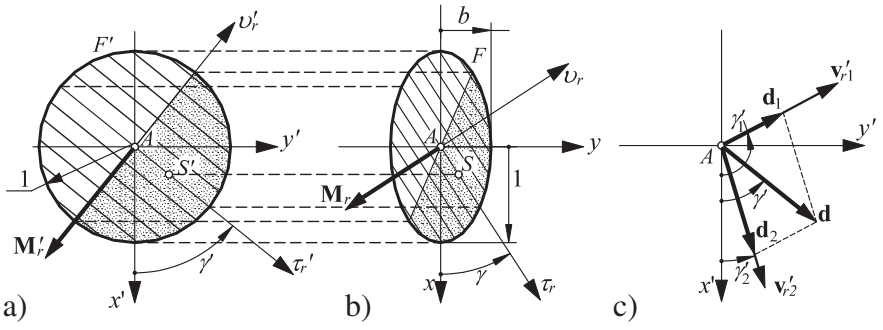

Fig. 3. Elliptic contact area between two bodies with the coordinate systems.

opposes angular velocity $\boldsymbol{\omega}'_r$ of the rolling, i.e. $\mathbf{M}'_r = -M'_r\boldsymbol{\omega}'_r/\|\boldsymbol{\omega}'_r\|$, therefore they represent a rather classical approach to the rolling friction. However, this way of understanding of the rolling resistance can lead in certain cases to cumbersome and questionable results (Leine, 2009; Leine et al., 2005; Leine and Van De Wouw, 2008). If we, for example, consider the case of two bodies moving over each other with no relative angular velocity, contact point A still moves over the surfaces of both bodies. The classical approach to the rolling resistance results in no dissipation in this case, which is not true. Therefore, a certain group of researchers (Leine, 2009; Leine et al., 2005; Leine and Van De Wouw, 2008) replace the classical rolling friction model by the concept of contour friction as a resistance against relative movement of the contact point over the body surface. This movement can be different for each body (and the contour friction can also be different) and is defined by contour velocities $\mathbf{v}'_{r1}$ and $\mathbf{v}'_{r2}$. The classical rolling resistance and contour friction models lead to the same results in certain special cases (e.g. in rolling without sliding or in the case of rolling of a deformable body over the rigid plane), but in general they differ essentially one from the other. However, the proposed model of contour friction does not take into account the shape of the contact region and coupling between rolling resistance and components of the friction model (by a proper model of normal stress distribution over the contact area).

Going back to model (15) and Fig. 3a, we will rather use the concept closely related to the contour friction. It means that the axis τ'_r corresponds to the direction of the velocity of relative motion (contour velocity) of point A over the body. Let us assume now, temporarily, that only one such direction exists, i.e. directions of $\mathbf{v}'_{r1}$ and $\mathbf{v}'_{r2}$ coincide (the case of rolling without sliding) or only one of them is significant (the case when, for example, only one of the bodies undergoes deformation at the contact region). Now, the distortion in normal stress distribution (15) along the direction τ'_r can be explained, to a certain extent, by the dissipation processes proceeding in the deformed material. Assuming function $\sigma'_0(\rho')$ to be decreasing, we can note that on the leading half of the contact (dotted region in Fig. 3a), where the nominal normal stress σ'_0 increases in time (we can say that the strain energy of material elements increases due to the work of compression done by the contact pressure), the actual normal stress σ' is greater than σ'_0. On the rest of the contact region, where the nominal normal stress σ'_0 decreases in time, the actual normal stress σ' is smaller than σ'_0 and we can talk of the process of unloading.

For the constant value of parameter d, the rolling resistance torque $\mathbf{M}'_r$ does not depend on the contour velocity and its dimensional counterpart $\widehat{\mathbf{M}}'_r = \widehat{a}\widehat{N}\mathbf{M}'_r$ is proportional to the dimensional radius of contact $\widehat{a}$ and dimensional normal load $\widehat{N}$. The last effect is consistent with the results obtained assuming the hypothesis of the so-called *elastic hysteresis* (Greenwood et al., 1961; Johnson, 1985; Tabor, 1955), i.e. the simplified theory of dissipation processes proceeding in the deformed material within the so-called elastic limit. In this theory the energy loss is expressed as a certain fraction α of the maximum elastic strain energy stored in the body during the cycle of loading and unloading. Then assuming rolling with the frictionless Hertz contacts of line (e.g. a cylinder rolling over the plane) or elliptic (or circular) shape they calculate the strain energy from the work done by the contact pressure on the leading part of the contact. It results in a simple rolling theory where resistance torque is proportional to normal load and contact size in the direction of the deformation region motion. These results are then confirmed experimentally quite well, especially for materials such as rubber. The other mechanisms of rolling resistance, such as micro-slips and roughness of the surfaces usually play a much less important role (Johnson, 1985). A bit greater errors of the assumed model of rolling resistance can arise from a different than assumed mechanism of energy dissipation during inelastic deformation of the material.

Now, we will try to extend the model of distorted distribution of normal stress (15) on circular area to the corresponding model on elliptic zone. We do it by the contraction of area F' (see Fig. 3) along y' axis. We obtain elliptic area F shown in Fig. 3b, where the position of each point is determined by the use of coordinates x and y of rectangular coordinate system Axy. The relations between coordinates of each point of the contact area before (x', y') and after contraction (x, y) are $x = x'$ and $y = by'$, respectively. The dimensionless quantities used in Fig. 3 are $a = \widehat{a}/\widehat{a} = 1$ and $0 < b = \widehat{b}/\widehat{a} \leq 1$, where $\widehat{a}$ is the real characteristic dimension of the contact zone (in this case it is the real length of the major semi-axis of the elliptic contact).

The dimensionless normal stress distribution $\sigma(x,y) = b^{-1}\sigma'(x, b^{-1}y)$ over the area $F(\iint_F \sigma \mathrm{d}F = \iint_F \sigma_0 \mathrm{d}F = 1)$ equals

$$\begin{aligned} &\sigma(x,y) = \sigma_0(x,y)(1 + dx\cos\gamma' + db^{-1}y\sin\gamma'), \\ &\text{where } \sigma_0(x,y) = b^{-1}\sigma'_0\left(\sqrt{x^2 + b^{-2}y^2}\right). \end{aligned} \tag{16}$$

Together with the contraction of the contact area, the direction of contour velocity changes from τ'_r to τ_r. Thanks to it (assuming function $\sigma'_0(\rho')$ to be decreasing) the dotted region in Fig. 3b, where the actual stress σ is greater than the nominal one σ_0, is also the leading part of the contact, i.e. nominal stress σ_0 is increasing in time (the process of loading takes place). Note however, that we do not take into account the relative rotation of the deformed region (angular contour velocity) and its influence on the normal stress distribution and rolling resistance. The relation between angles γ' and γ reads

$$\cos\gamma' = \frac{\cos\gamma}{\sqrt{\cos^2\gamma + b^{-2}\sin^2\gamma}}, \quad \sin\gamma' = \frac{b^{-1}\sin\gamma}{\sqrt{\cos^2\gamma + b^{-2}\sin^2\gamma}}. \tag{17}$$

On the other hand, the movement direction of deformation zone F is different for each body (with the exception of the case of rolling without sliding, or when only one of the bodies undergoes deformation at contact region), so there are two different contour velocities $\mathbf{v}_{r1}$ and $\mathbf{v}_{r2}$ (and also $\mathbf{v}'_{r1}$ and $\mathbf{v}'_{r2}$) with two different coefficients d_1 and d_2. We can assume a model in which total distortion of the normal stress distribution is the sum of distortions related to contour resistances on each body separately

$$\begin{aligned} \sigma(x,y) = \sigma_0(x,y)\Bigg(1 + \underbrace{(d_1\cos\gamma'_1 + d_2\cos\gamma'_2)}_{d_c = d\cos\gamma'}\, x \\ + b^{-1}\underbrace{(d_1\sin\gamma'_1 + d_2\sin\gamma'_2)}_{d_s = d\sin\gamma'}\, y\Bigg), \end{aligned} \tag{18}$$

where d and γ' are the corresponding parameters of the resultant resistance. One can note that Eq. (16) is still valid and the resultant resistance can be understood as geometric sum $\mathbf{d} = \mathbf{d}_1 + \mathbf{d}_2$, where $\mathbf{d}_1 = d_1\mathbf{v}'_{r1}/\|\mathbf{v}'_{r1}\|$ and $\mathbf{d}_2 = d_2\mathbf{v}'_{r2}/\|\mathbf{v}'_{r2}\|$ and where vector $\mathbf{d}$ has magnitude d (see Fig. 3c). In order to simplify the notation, we have omitted the prime sign $(\ldots)'$ in relation to vectors $\mathbf{d}$, $\mathbf{d}_1$ and $\mathbf{d}_2$. Quantities γ'_1 and γ'_2 occurring in Eq. (18) denote the angles between the x' axis and the directions of velocities $\mathbf{v}'_{r1}$ and $\mathbf{v}'_{r2}$ (or vectors $\mathbf{d}_1$ and $\mathbf{d}_2$), respectively. The condition of non-negative values of normal stresses now gets the form $d_1 + d_2 \leq 1$, where $d_1 > 0$ and $d_2 > 0$ (resistance should dissipate energy).

In practice, it is convenient to determine components d_c and d_s of expression (18) in the following way

$$\begin{aligned} d_c &= d_1\cos\gamma_1' + d_2\cos\gamma_2', \\ d_s &= d_1\sin\gamma_1' + d_2\sin\gamma_2', \end{aligned} \tag{19}$$

where

$$\begin{aligned} \cos\gamma_1' &= \frac{v_{r1x}}{\sqrt{v_{r1x}^2+b^{-2}v_{r1y}^2}}, \quad \sin\gamma_1' = \frac{b^{-1}v_{r1y}}{\sqrt{v_{r1x}^2+b^{-2}v_{r1y}^2}}, \\ \cos\gamma_2' &= \frac{v_{r2x}}{\sqrt{v_{r2x}^2+b^{-2}v_{r2y}^2}}, \quad \sin\gamma_2' = \frac{b^{-1}v_{r2y}}{\sqrt{v_{r2x}^2+b^{-2}v_{r2y}^2}}, \end{aligned} \tag{20}$$

and where $v_{r1x} = v'_{r1x'}$, $v_{r1y} = bv'_{r1y'}$, $v_{r2x} = v'_{r2x'}$ and $v_{r2y} = bv'_{r2y'}$ are the components of the contour velocities $\mathbf{v}_{r1} = v_{r1x}\mathbf{e}_x + v_{r1y}\mathbf{e}_y$ and $\mathbf{v}_{r2} = v_{r2x}\mathbf{e}_x + v_{r2y}\mathbf{e}_y$ in the coordinate system Axy, where $v'_{r1x'}$, $v'_{r1y'}$, $v'_{r2x'}$ and $v'_{r2y'}$ are the components of the corresponding velocities $\mathbf{v}'_{r1} = v'_{r1x'}\mathbf{e}_{x'} + v'_{r1y'}\mathbf{e}_{y'}$ and $\mathbf{v}'_{r2} = v'_{r2x'}\mathbf{e}_{x'} + v'_{r2y'}\mathbf{e}_{y'}$ in the coordinate system $Ax'y'$. Since the corresponding real velocities $\widehat{\mathbf{v}}_{r1} = \alpha\widehat{a}\mathbf{v}_{r1}$ and $\widehat{\mathbf{v}}_{r2} = \alpha\widehat{a}\mathbf{v}_{r2}$ have the same directions as non-dimensional ones, non-dimensional components in Eq. (20) can be replaced by real ones.

In the process of integration of the functions of type $f(x,y)\sigma(x,y)$ over the elliptic contact area F, it is convenient to use polar coordinate system (r,φ), where $x = x' = \rho'\cos\varphi$ and $y = by' = b\rho'\sin\varphi$. Then, we obtain

$$\begin{aligned} \iint_F f(x,y)\sigma(x,y)\mathrm{d}x\mathrm{d}y &= \iint_{F'} f(x',by')\sigma'(x',y')\mathrm{d}x'\mathrm{d}y' \\ &= \int_0^{2\pi}\int_0^1 f(\rho'\cos\varphi, b\rho'\sin\varphi)\sigma_0'(\rho')(1 + d\cos\gamma'\rho'\cos\varphi \\ &\quad + d\sin\gamma'\rho'\sin\varphi)\rho'\mathrm{d}\rho'\mathrm{d}\varphi \\ &= \int_0^{2\pi}\int_0^1 f(\rho'\cos\varphi, b\rho'\sin\varphi)\sigma_0'(\rho')(1 + d\rho'\cos(\varphi-\gamma'))\rho'\mathrm{d}\rho'\mathrm{d}\varphi. \end{aligned} \tag{21}$$

Position S of the centre of normal stress distribution $\sigma(x,y)$ over non-dimensional area F reads

$$x_S = \frac{\iint_F \sigma(x,y)x\mathrm{d}F}{\iint_F \sigma(x,y)\mathrm{d}F} = \pi I_3 d_c, \quad y_S = \frac{\iint_F \sigma(x,y)y\mathrm{d}F}{\iint_F \sigma(x,y)\mathrm{d}F} = \pi b I_3 d_s, \tag{22}$$

where I_3 belongs to the following family of the parameters

$$I_i = \int_0^1 \sigma_0'(\rho')\rho'^i\mathrm{d}\rho'. \tag{23}$$

It results from Eqs. (17) and (22) that $x_s/y_s = \tan\gamma$ and point S lies on the $A\tau_r$.

Let us introduce vector $\mathbf{f} = f_x\mathbf{e}_x + f_y\mathbf{e}_y = f\mathbf{e}_{\tau_r}$, where $f_x = x_S$, $f_y = y_S$ and $f = \sqrt{f_x^2+f_y^2} = AS$. Then we can obtain the non-dimensional rolling resistance torque from equation $\mathbf{M}_r = \mathbf{f}\times\mathbf{N}$, where $\mathbf{N} = \mathbf{e}_z$ is the non-dimensional normal reaction, which takes the following form

$$\mathbf{M}_r = y_s\mathbf{e}_x - x_s\mathbf{e}_y. \tag{24}$$

Real rolling friction torque reads $\widehat{\mathbf{M}}_r = \widehat{a}\widehat{N}\mathbf{M}_r$, where $\widehat{a}$ is the real characteristic dimension of the contact and $\widehat{N}$ is the real resultant normal reaction. Real and dimensionless rolling friction torques can also be expressed as $\mathbf{M}_r = -f\mathbf{e}_{v_r}$ and $\widehat{\mathbf{M}}_r = -\widehat{f}\mathbf{e}_{v_r}$, where $\widehat{f} = \widehat{a}\widehat{N}f$ is the real rolling friction coefficient understood classically as a shift of the point of application of normal reaction force.

Let us note that rolling resistance defined by Eq. (24) with consideration of formulae (22) and (19), with the assumption of constant values of coefficients d_1 and d_2, in the case of movement of the deformation zone along one of the axes of contact ($\gamma_1' = \gamma_2' = i\pi/2$, where $i\in C$), is proportional to the length of that axis. It is consistent with the earlier discussed experimental and theoretical results based on the hypothesis of elastic hysteresis (Greenwood et al., 1961; Johnson, 1985; Tabor, 1955).

On the other hand, we would like to extend the above model and have a possibility to investigate orthotropic properties of rolling resistance independently of parameter b describing the shape of contact area. It would facilitate an investigation of certain properties of coupled friction and rolling resistance model, e.g. the investigation of a friction model with circular contact area but rolling resistance different along two perpendicular directions. We wish to develop but at the same time to maintain validity of all above equations and properties of the pressure distribution and rolling resistance model.

Vector $\mathbf{f} = x_S\mathbf{e}_x + y_S\mathbf{e}_y$ defining the position of centre S of normal stress distribution, after consideration of Eqs. (22) and (19), can be expressed as the sum $\mathbf{f} = \mathbf{f}_1 + \mathbf{f}_2 = (f_{1x}+f_{2x})\mathbf{e}_x + (f_{1y}+f_{2y})\mathbf{e}_y$ (see Fig. 4), where vectors $\mathbf{f}_1 = f_{1x}\mathbf{e}_x + f_{1y}\mathbf{e}_y$ and $\mathbf{f}_2 = f_{2x}\mathbf{e}_x + f_{2y}\mathbf{e}_y$ include the following components in the Axy coordinate system

$$\begin{aligned} f_{1x} &= \pi I_3 d_1\cos\gamma_1', \quad f_{1y} = \pi b I_3 d_1\sin\gamma_1', \\ f_{2x} &= \pi I_3 d_2\cos\gamma_2', \quad f_{2y} = \pi b I_3 d_2\sin\gamma_2' \end{aligned} \tag{25}$$

and define the position of centre of the normal stress distribution for $d_2 = 0$ (point S_1) and $d_1 = 0$ (point S_2) respectively. Let us note that for constant values of d_1 and d_2, points S_1 and S_2 move on elliptic trajectories of eccentricities equal to the eccentricity of contact area F. Moreover, these points lie on $A\tau_{r1}$ and $A\tau_{r2}$ axes of directions defined by velocities $\mathbf{v}_{r1}$ and $\mathbf{v}_{r2}$, respectively ($f_{1x}/f_{1y} = v_{r1x}/v_{r1y}$ and $f_{2x}/f_{2y} = v_{r2x}/v_{r2y}$), which can be proved easily by the use of Eqs. (25) and (20).

Now, we would like to change the eccentricities of trajectories of points S_1 and S_2, however preserving the condition that these points lie on $A\tau_{r1}$ and $A\tau_{r2}$ axes, respectively. One can do that by the modelling of rolling resistance coefficients d_1 and d_2 as functions of γ_1 and γ_2 angles

$$\begin{aligned} d_1\cos\gamma_1' &= d_{a1}\cos\gamma_1'', \quad d_1\sin\gamma_1' = b_1 d_{a1}\sin\gamma_1'', \\ d_2\cos\gamma_2' &= d_{a2}\cos\gamma_2'', \quad d_2\sin\gamma_2' = b_2 d_{a2}\sin\gamma_2'', \end{aligned} \tag{26}$$

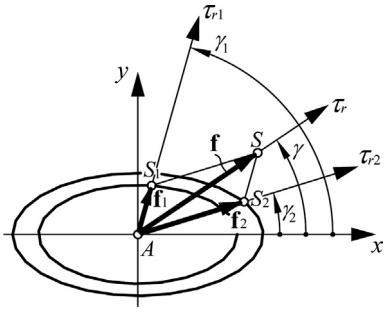

Fig. 4. Geometric interpretation of rolling resistances' superposition.

where

$$\cos\gamma_1'' = \frac{v_{r1x}}{\sqrt{v_{r1x}^2+b^{-2}b_1^{-2}v_{r1y}^2}},\quad \sin\gamma_1'' = \frac{b^{-1}b_1^{-1}v_{r1y}}{\sqrt{v_{r1x}^2+b^{-2}b_1^{-2}v_{r1y}^2}},$$
$$\cos\gamma_2'' = \frac{v_{r2x}}{\sqrt{v_{r2x}^2+b^{-2}b_2^{-1}v_{r2y}^2}},\quad \sin\gamma_2'' = \frac{b^{-1}b_2^{-1}v_{r2y}}{\sqrt{v_{r2x}^2+b^{-2}b_2^{-1}v_{r2y}^2}}, \tag{27}$$

and where d_{a1}, $d_{b1} = b_1 d_{a1}$, d_{a2} and $d_{b2} = b_2 d_{a2}$ are the constant coefficients of rolling resistance for bodies 1 and 2, in directions x and y, respectively. Parameters b_1 and b_2 define the change of eccentricities of the trajectories of points S_1 and S_2 with respect to the eccentricity of contact area F. The corresponding coordinates of vectors $\mathbf{f}_1$ and $\mathbf{f}_2$ read

$$f_{1x} = \pi I_3 d_{a1}\cos\gamma_1'',\quad f_{1y} = \pi b I_3 b_1 d_{a1}\sin\gamma_1'',$$
$$f_{2x} = \pi I_3 d_{a2}\cos\gamma_1'',\quad f_{2y} = \pi b I_3 b_2 d_{a2}\sin\gamma_2'' \tag{28}$$

and one can check, using Eqs. (28) and (27), that $f_{1x}/f_{1y} = v_{r1x}/v_{r1y}$ and $f_{2x}/f_{2y} = v_{r2x}/v_{r2y}$.

As we have noted, all relations and elements of rolling resistance and pressure distribution modelling presented in the current subsection remain valid. Rolling resistance torque is determined by relations (24) and (22), where quantities d_c and d_s are defined by formulae (19). It is convenient to use these equations when $b_1 = b_2 = 1$, because it follows from Eqs. (20), (27) and (26) that $\gamma_1'' = \gamma_1'$, $\gamma_2'' = \gamma_2'$ and the rolling resistance coefficients $d_1 = d_{a1} = d_{b1}$ and $d_2 = d_{a2} = d_{b2}$ are constant. In the opposite case, when quantities d_1 and d_2 are variable, one should use Eqs. (26) and (19) to obtain

$$d_c = d\cos\gamma' = d_{a1}\cos\gamma_1'' + d_{a2}\cos\gamma_2'',$$
$$d_s = d\sin\gamma' = b_1 d_{a1}\sin\gamma_1'' + b_2 d_{a2}\sin\gamma_2'', \tag{29}$$

where the functions of angles γ_1'' and γ_2'' are defined by Eq. (27). The condition of non-negative normal stresses takes the form $d_{a1} + d_{a2} \le 1$ and $d_{b1} + d_{b2} \le 1$, where $d_{a1} > 0$, $d_{b1} > 0$, $d_{a2} > 0$ and $d_{b2} > 0$.

Finally, let us note that rolling resistance for certain $b < 1$ and $b_1 = b_2 = 1$, can be replaced by model with $b = 1$, but with $b_1 = b_2 < 1$ having earlier value of b. That property enables investigation of the friction model with circular contact area but with orthotropic rolling friction model.

Fig. 5a illustrates normal stress distribution $\sigma(x,y)$ over the elliptic area ($b = 0.5$) resulting from distortion of Hertz distribution $\sigma_0(x,y) = 3/2\pi b\sqrt{1-x^2-b^{-2}y^2}$ $\left(\text{for } \sigma'_0(\rho') = \frac{3}{2\pi}\sqrt{1-\rho'^2}\right)$ being a result of coupling with rolling resistance ($d = 1$ and $\gamma' = \pi/4$). Fig. 5b exhibits sections of the stress distribution along direction of relative movement of the contact point (along axis τ_r, defined by angle γ, such, that $\cos\gamma = \cos\gamma'/\sqrt{\cos^2\gamma' + b^2\sin\gamma'}$ and $\sin\gamma = b\sin\gamma'/\sqrt{\cos^2\gamma' + b^2\sin\gamma'}$) for two different values of coordinate $v_r = 0$ and 0.5. The sections of the distorted stress distribution $\sigma(x,y)$ are compared to the corresponding sections of stress distribution before deformation $\sigma_0(x,y)$. The use of angle γ' in expression (16) instead of angle γ (which one could consider more intuitive) would violate the rule stating that where during movement of the deformation zone the relative nominal displacement of the point grows (stress $\sigma_0(x,y)$ grows), stress $\sigma(x,y)$ is greater than stress $\sigma_0(x,y)$. It is well seen in Fig. 5b, where plots of stresses $\sigma(x,y)$ and $\sigma_0(x,y)$ cross each other in the points of maximum stress $\sigma_0(x,y)$ along corresponding section (because the direction of sections is one of the relative resultant movement of the deformation zone).

3.2. Integral model of friction

For stress distribution over the elliptic contact area defined by formulae (16), the parameters $c_{i,j,k}^{(x,y)}$ (according to Eq. (13)) of the exact integral model of friction, take the following form

$$c_{i,j,k}^{(x,y)} = b^j \int_0^{2\pi}\int_0^1 \rho'^{1+i+j-k}\sigma'_0(\rho')\frac{1+\rho' d\cos(\varphi-\gamma')}{\left(\cos^2\varphi + b^2\sin^2\varphi\right)^{k/2}} \times \cos^i\varphi\,\sin^j\varphi\,\mathrm{d}\rho'\,\mathrm{d}\varphi, \tag{30}$$

expressed in the polar coordinate system (ρ', φ) (see Eq. (21)). The integrals $c_{i,j,k}^{(x,y)}$ can be calculated analytically and some most important examples are presented in Table 1 in Appendix B. However full expressions for friction forces and moment are difficult to express in analytical form.

Fig. 6 shows the surfaces in space (T_{sx}, T_{sy}, M_s), defined parametrically by functions (10) of the integral model of friction for normal stress distribution before distortion determined by Hertz theory ($\sigma'_0(\rho') = 3/2\pi\sqrt{1-\rho'^2}$), for different values of parameters b and d. The exhibited surfaces correspond to sliding state of contact and they are obtained by the use of numerical integration of functions (10) for parameters $\varphi_s \in \langle 0, 2\pi\rangle$ and $\theta_s \in \langle 0, \pi\rangle$. The dashed lines connecting points of constant values of parameter φ_s meet each other in two points. One of them marked in orange (in the web version) is visible in the plots and corresponds to parameter $\theta_s = \pi/2$. The second one (invisible) corresponds to parameter $\theta_s = -\pi/2$. Both points correspond to the non-zero positive (for the first point) or negative (for the second point) value of ω_s with $v_s = 0$. The zones bounded by the surfaces and containing the origin of the coordinate system correspond to the stick mode, when

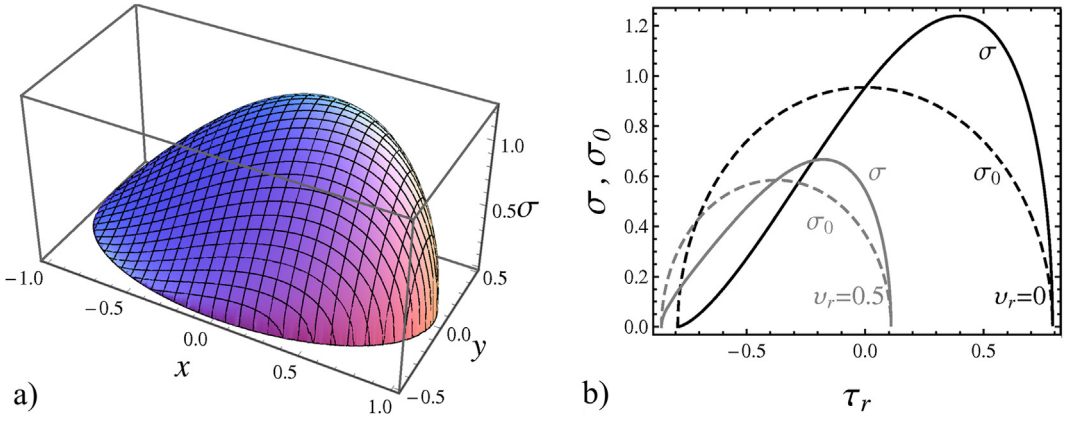

Fig. 5. Distorted Hertz stress distribution $\sigma(x,y)$ over elliptic contact for parameters $b = 0.5$, $d = 1$ and $\gamma' = \pi/4$ (a) and its sections along direction of relative movement of the contact point compared to the corresponding stress distribution $\sigma_0(x,y)$ before distortion (b).

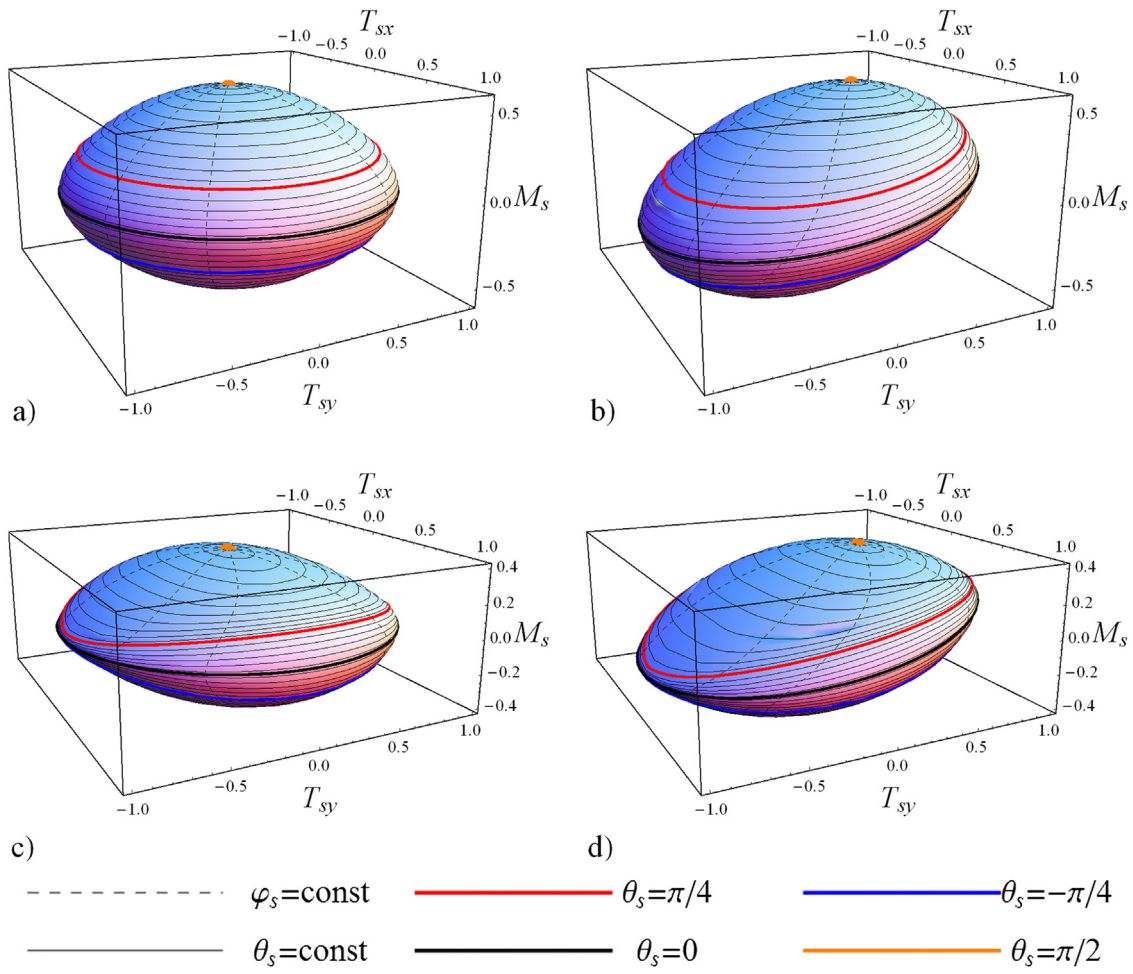

Fig. 6. Surfaces of integral friction model components (10) in space (T_{sx}, T_{sy}, M_s) for different eccentricities of elliptic contact and rolling resistance coefficient and with the assumption of model (16) of normal stress distribution for $\sigma_0'(r) = 3/2\pi\sqrt{1-r^2}$: a) $b = 1$, $d = 0$; b) $b = 1$; $d = 1$, $\gamma' = 0$; c) $b = 0.3$; $d = 0$; d) $b = 0.3$; $d = 1$; $\gamma' = 0$.

relative motion of the contact patch disappears (relative motion of the bodies can still take place as a result of rolling) and components of the friction model result from certain equilibrium conditions of the interacting bodies.

Fig. 7 shows sections $M_s = 0$, $T_{sx} = 0$ and $T_{sy} = 0$ of the corresponding surfaces exhibited by Fig. 6, where additionally the solutions for two different rolling directions $\gamma' = 0$ and $\gamma' = \pi/2$ are plotted. One can observe, that for the lack of rolling resistance ($d = 0$), the section in $M_s = 0$ plane has a circular shape independently of the value of parameter b.

A numerical construction of the boundaries of areas shown in Fig. 7 was performed by the use of parametric functions in the polar coordinate system. For example, curves in the T_{sy}–M_s coordinate system are determined by functions $T_{sy}(\varphi_x) = r_{yz}(\varphi_x)\cos\varphi_x$ and $M_s(\varphi_x) = r_{yz}(\varphi_x)\sin\varphi_x$, where for each value $\varphi_x \in \langle 0, 2\pi)$, radius $r_{yz}(\varphi_x)$ is computed numerically from the set of equations

$$\begin{aligned} T_{sx}(\varphi_s, \theta_s) &= 0, \\ T_{sy}(\varphi_s, \theta_s) &= r_{yz}(\varphi_x)\cos\varphi_x, \\ M_s(\varphi_s, \theta_s) &= r_{yz}(\varphi_x)\sin\varphi_x, \end{aligned} \tag{31}$$

where the left-hand side of the equations is determined by the model (10). Assuming that $r_{yz}(\varphi_x) > 0$, the above system has always only one solution with respect to variables φ_s, θ_s and r_{yz}. Computation of the corresponding curves in other sections is performed in an analogical way.

4. Approximations of the integral model of friction

Since the analytical solutions to exact integral model (8) are difficult to find or do not exist, we will look for appropriate approximate models. The simplest possible approximation of integral model is the one ignoring the coupling between friction force and torque (that is assuming a point contact in relation to friction force, but non-zero friction torque)

$$\mathbf{T}_s^{(O)} = -\frac{\mathbf{v}_s}{\|\mathbf{v}_s\|}, \quad \mathbf{M}_s^{(O)} = -\frac{\boldsymbol{\omega}_s}{\|\boldsymbol{\omega}_s\|}, \tag{32}$$

where superscript (O) is used to denote a specific kind of approximation. Although both dimensionless friction force $\mathbf{T}_s^{(O)}$ and torque $\mathbf{M}_s^{(O)}$ are assumed to have magnitudes equal to 1 (for $\|\mathbf{v}_s\| \neq 0$ and $\|\boldsymbol{\omega}_s\| \neq 0$, respectively), their real counterparts are determined independently by two parameters μ and $\widehat{a}$ (see Sect. 2). Since $\mathbf{v}_s = v_s\cos\varphi_s\mathbf{e}_x + v_s\sin\varphi\mathbf{e}_y$, $\boldsymbol{\omega}_s = \omega_s\mathbf{e}_z$, $\mathbf{T}_s^{(O)} = -T_{sx}^{(O)}\mathbf{e}_x - T_{sy}^{(O)}\mathbf{e}_y$ and $\mathbf{M}_s^{(O)} = -M_s^{(O)}\mathbf{e}_z$, from (32) we obtain the following non-dimensional model

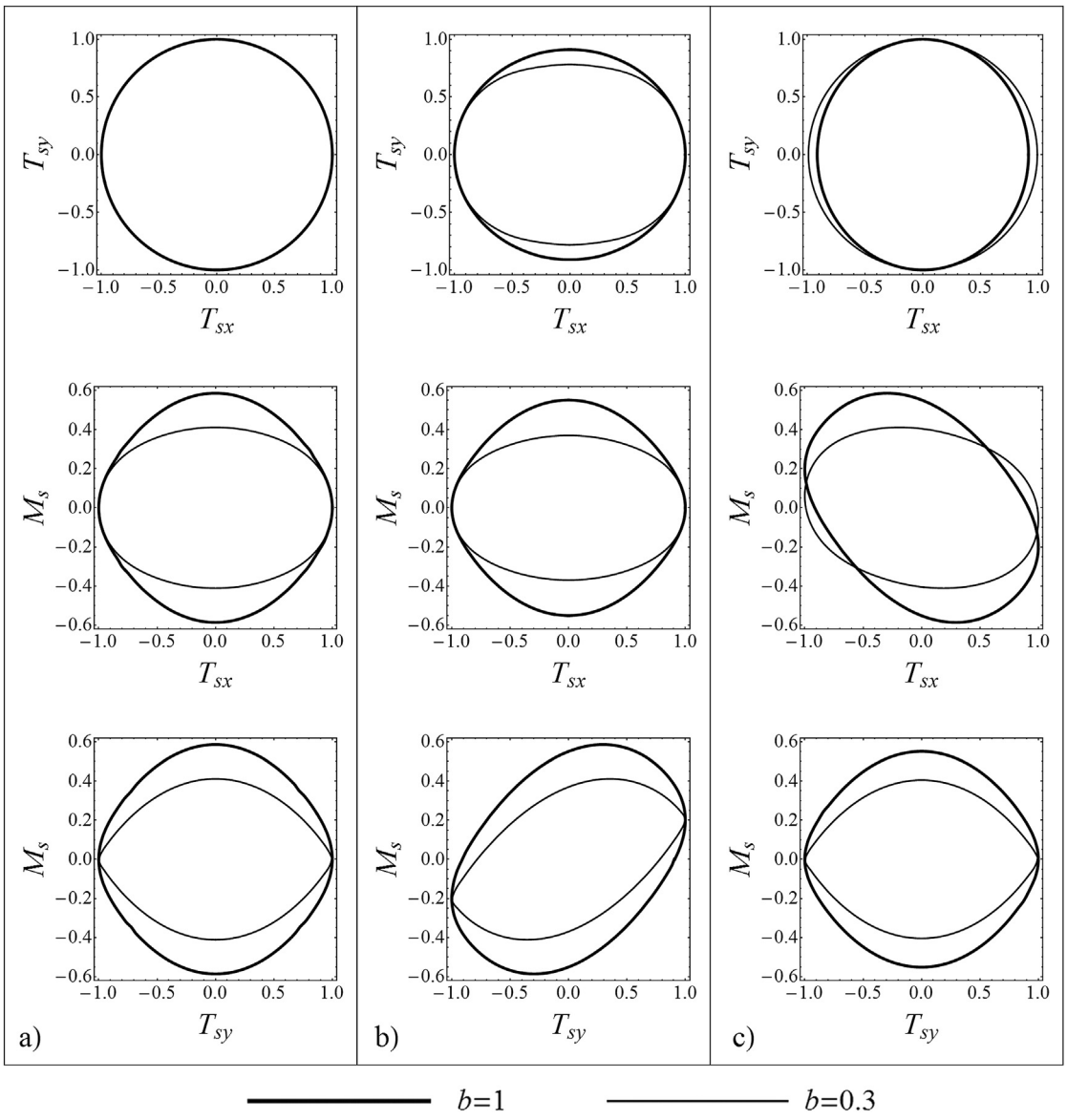

Fig. 7. Components of integral friction model (10) in sections $M_s = 0$, $T_{sx} = 0$ and $T_{sy} = 0$: a) $d = 0$; b) $d = 1$, $\gamma' = 0$; c) $d = 1$, $\gamma' = \pi/2$. Normal stress distribution corresponds to model (16) for $\sigma'_0(r) = 3/2\pi\sqrt{1-r^2}$.

$$T_{sx}^{(O)} = \cos\varphi_s, \quad T_{sy}^{(O)} = \sin\varphi_s, \quad M_s^{(O)} = \operatorname{sgn}(\omega_s). \tag{33}$$

4.1. Padé approximations and their modifications

Let as try to assume the following general form of the n_f order Padé approximation to f component of the integral friction model (8)

$$f^{\left(P_{n_f}\right)}(v_s,\omega_s,\varphi_s) = \frac{\sum_{i=0}^{n_f} a_{f,i} v_s^{n_f-i}\omega_s^i}{\sum_{i=0}^{n_f} b_{f,i} v_s^{n_f-i}\omega_s^i}, \quad \text{where } f = T_{sx},\ T_{sy},\ M_s, \tag{34}$$

and where $b_{f,0} = 1$, $a_{f,i} = a_{f,i}(\varphi_s, \operatorname{sgn}(v_s), \operatorname{sgn}(\omega_s))$, $b_{f,i} = b_{f,i}(\varphi_s, \operatorname{sgn}(v_s), \operatorname{sgn}(\omega_s))$ and where the dependence of the components and coefficients on the normal stress distribution in the Axy coordinate system is omitted for brevity. One can easily check, that using relations (9), the above approximation can be reduced to the function of variables φ_s and θ_s, similarly like the full integral model (10). In fact, all Padé approximations developed in works (Kireenkov, 2005, 2008; Zhuravlev, 1998, 2003) are special cases of their general form (34).

Let us introduce the following alternative notation of approximant (34)

$$f^{\left(P_{n_{f1}}\left(n'_{f1}\right),n_{f2}\left(n'_{f2}\right)\right)}(v_s,\omega_s,\varphi_s) = \frac{\sum_{i=0}^{n_f} a_{f,i} v_s^{n_f-i}\omega_s^i}{\sum_{i=0}^{n_f} b_{f,i} v_s^{n_f-i}\omega_s^i}, \quad \text{for } f = T_{sx},\ T_{sy},\ M_s, \tag{35}$$

meaning, that the coefficients of the above approximants fulfil the following set of conditions

$$\begin{aligned}
&\left.\frac{\partial^i f^{\left(P_{n_f}\right)}}{\partial v_s^i}\right|_{v_s=0} = \left.\frac{\partial^i f}{\partial v_s^i}\right|_{v_s=0} \quad \text{for } i = 0,\ldots,n'_{f1},\\
&\left.\frac{\partial^i f^{\left(P_{n_f}\right)}}{\partial v_s^i}\right|_{v_s=0} = 0 \quad \text{for } i = n'_{f1}+1,\ldots,n_{f1},\\
&\left.\frac{\partial^i f^{\left(P_{n_f}\right)}}{\partial \omega_s^i}\right|_{\omega_s=0} = \left.\frac{\partial^i f}{\partial \omega_s^i}\right|_{\omega_s=0} \quad \text{for } i = 0,\ldots,n'_{f2},\\
&\left.\frac{\partial^i f^{\left(P_{n_f}\right)}}{\partial \omega_s^i}\right|_{\omega_s=0} = 0 \quad \text{for } i = n'_{f2}+1,\ldots,n_{f2},
\end{aligned} \tag{36}$$

and where $f = T_{sx}, T_{sy}, M_s$, $n_f = (n_{f1}+n_{f2}+1)/2$, $n_{f1} \geq n'_{f1}$ and $n_{f2} \geq n'_{f2}$. In the case of $n_{f1} = n'_{f1}$ or $n_{f2} = n'_{f2}$ we omit the corresponding index in the parenthesis.

For $n_{T_{sx}} = n_{T_{sy}} = n_{M_s} = 1$, from (34) we get the following Padé approximations of first order

$$f^{(P_1)} = \frac{a_{f,0}v_s + a_{f,1}\omega_s}{v_s + b_{f,1}\omega_s}, \quad \text{where } f = T_{sx},\ T_{sy},\ M_s. \tag{37}$$

Then making use of Eqs. (11) and (59)–(61), we find the following coefficients of the above approximants for $n_{T_{sx}1} = n_{T_{sy}1} = n'_{T_{sx}1} = n'_{T_{sy}1} = n_{M_s2} = n'_{M_s2} = 1$ and $n_{T_{sx}2} = n_{T_{sy}2} = n'_{T_{sx}2} = n'_{T_{sy}2} = n_{M_s1} = n'_{M_s1} = 0$:

$$\begin{aligned}
&a_{T_{sx},0} = c_\varphi \operatorname{sgn}(v_s), \quad a_{T_{sx},1} = -\operatorname{sgn}(v_s)c^{(x,y)}_{0,1,1}A_1, \quad b_{T_{sx},1} = \operatorname{sgn}(v_s)\operatorname{sgn}(\omega_s)A_1,\\
&a_{T_{sy},0} = \operatorname{sgn}(v_s)s_\varphi, \quad a_{T_{sy},1} = \operatorname{sgn}(v_s)c^{(x,y)}_{1,0,1}A_2, \quad b_{T_{sy},1} = \operatorname{sgn}(v_s)\operatorname{sgn}(\omega_s)A_2,\\
&a_{M_s,0} = 1, \quad a_{M_s,1} = \operatorname{sgn}(v_s)c^{(x,y)}_{0,0,-1}A_3^{-1}A_4^{-1}, \quad b_{M_s,1} = \operatorname{sgn}(v_s)\operatorname{sgn}(\omega_s)A_4^{-1},
\end{aligned} \tag{38}$$

where

$$\begin{aligned}
&A_1 = \frac{c_\varphi + \operatorname{sgn}(v_s)\operatorname{sgn}(\omega_s)c^{(x,y)}_{0,1,1}}{c^{(x,y)}_{1,1,3}s_\varphi + c^{(x,y)}_{2,0,3}c_\varphi}, \quad A_2 = \frac{s_\varphi - \operatorname{sgn}(v_s)\operatorname{sgn}(\omega_s)c^{(x,y)}_{1,0,1}}{c^{(x,y)}_{0,2,3}s_\varphi + c^{(x,y)}_{1,1,3}c_\varphi},\\
&A_3 = c^{(x,y)}_{1,0,0}s_\varphi - c^{(x,y)}_{0,1,0}c_\varphi, \quad A_4 = \frac{\operatorname{sgn}(v_s)c^{(x,y)}_{0,0,-1} - \operatorname{sgn}(\omega_s)A_3}{\left(c^{(x,y)}_{0,2,0} - c^{(x,y)}_{2,0,0}\right)s_\varphi^2 + 2c^{(x,y)}_{1,1,0}c_\varphi s_\varphi + c^{(x,y)}_{2,0,0}}.
\end{aligned}$$

Making use of the above relations, from (37) we get the following form of the friction model

$$\begin{aligned}
&T_{sx}^{(P_{1,0})} = \frac{v_s c_\varphi - A_1 c^{(x,y)}_{0,1,1}\omega_s}{|v_s| + A_1|\omega_s|}, \quad T_{sy}^{(P_{1,0})} = \frac{v_s s_\varphi + A_2 c^{(x,y)}_{1,0,1}\omega_s}{|v_s| + A_2|\omega_s|},\\
&M_s^{(P_{0,1})} = \frac{c^{(x,y)}_{0,0,-1}\omega_s + A_3A_4v_s}{|\omega_s| + A_4|v_s|}.
\end{aligned} \tag{39}$$

One can note rather inconvenient form of approximant (39). It, however, will take a much simpler form in the case of circular contact area or constant elliptic shape. But there is another disadvantage of these models, namely the possible existence of singularities (the denominator tending to zero) for certain values of arguments and parameters. Much more convenient and free from the above drawback is the following construction of the approximation

$$f^{\left(I_{n_f}\right)}(v_s,\omega_s,\varphi_s) = \frac{\sum_{i=0}^{n_f} a_{f,i}v_s^{n_f-1}\omega_s^i}{\left(|v_s|^{m_f n_f} + b_f^{m_f}|\omega_s|^{m_f n_f}\right)^{m_f^{-1}}}, \quad \text{where}$$
$$f = T_{sx},\ T_{sy},\ M_s, \tag{40}$$

where $a_{f,i} = a_{f,i}(\varphi_s, \operatorname{sgn}(v_s), \operatorname{sgn}(\omega_s))$ (it occurs that for odd n_f, coefficients $a_{f,i}$ do not depend on the signs of v_s and ω_s), $m_f \geq 0$ and $b_f \geq 0$. In the above approximation we assume additionally, that $n_{T_{sx}} = n_{T_{sy}} = n_{T_s}$, $m_{T_{sx}} = m_{T_{sy}} = m_{T_s}$ and $b_{T_{sx}} = b_{T_{sy}} = b_{T_s}$. Thanks to that one can easily pass between different coordinate systems defined by rotation of the coordinate system *Axyz* around the axis *z* (see Fig. 1). In particular the structure of the model does not change during such a transformation (the denominator of the approximation does not change). Moreover, independently from the coordinate system chosen for derivation of the model, one always obtains the same structure of the friction model. The last property is related to the another one, that is for circularly symmetric contact stress distribution, independently from the choice of the coordinate system, one always obtain a model, where the friction force component perpendicular to the sliding velocity $\boldsymbol{v}_s$ is equal to zero (one can easy find that it true for full integral model).

Note, that for $m_f = 1$ we get the following particular form of Padé approximation (34)

$$f^{\left(I_{n_f}\right)}(v_s,\omega_s,\varphi_s)\Big|_{m_f=1} = \frac{\sum_{i=0}^{n_f} a_{f,i}v_s^{n_f-1}\omega_s^i}{|v_s|^{n_f} + b_f|\omega_s|^{n_f}}, \quad \text{where}$$
$$f = T_{sx},\ T_{sy},\ M_s, \tag{41}$$

and for $m_f = n_f^{-1}$ the next special form of expression (34)

$$f^{\left(I_{n_f}\right)}(v_s,\omega_s,\varphi_s)\Big|_{m_f=n_f^{-1}} = \frac{\sum_{i=0}^{n_f} a_{f,i}v_s^{n_f-1}\omega_s^i}{\left(|v_s| + b_f^{-n_f}|\omega_s|\right)^{n_f}}, \quad \text{where}$$
$$f = T_{sx},\ T_{sy},\ M_s. \tag{42}$$

Let us assume that the coefficients m_f and b_f are chosen arbitrarily and then the rest of the coefficients are chosen in such a way that the conditions (36) are fulfilled. Then it can be easily shown that for $i \leq n_f$ and $m_f \geq i/n_f$

$$\left.\frac{\partial^i f^{\left(I_{n_f}\right)}}{\partial v_s^i}\right|_{v_s=0} = i!\frac{a_{f,n_f-i}}{b_f}r_i(\omega_s), \quad \left.\frac{\partial^i f^{\left(I_{n_f}\right)}}{\partial \omega_s^i}\right|_{\omega_s=0} = i!a_{f,i}r_i(v_s), \tag{43}$$

where $r_i(x) = \begin{cases} x^{1-i}/|x| & \text{for } n = 1,3,5\ldots \\ x^{-i} & \text{for } n = 2,4,6\ldots \end{cases}$ and $i = 0,1,2\ldots n-1$.

Each of expressions (43) and each equation of type (36) contain only one unknown coefficient $a_{f,i}$, so the process of approximant

construction is much simplified. Moreover, the derivatives of approximant (40) do not depend on coefficient m_f.

Let us introduce the following alternative notation of approximant (40)

$$f^{\left(I_{n_{f1}\left(n'_{f1}\right),n_{f2}\left(n'_{f2}\right)}\right)}(v_s,\omega_s,\varphi_s) = \frac{\sum_{i=0}^{n_f} a_{f,i} v_s^{n_f-i}\omega_s^i}{\left(|v_s|^{m_f n_f}+b_f^{m_f}|\omega_s|^{m_f n_f}\right)^{m_f^{-1}}}, \quad \text{for}$$

$$f = T_{sx},\ T_{sy},\ M_s, \tag{44}$$

meaning that the coefficients of the above approximants fulfil the following set of conditions

$$\frac{\partial^i f^{\left(I_{n_f}\right)}}{\partial v_s^i}\Big|_{v_s=0} = \frac{\partial^i f}{\partial v_s^i}\Big|_{v_s=0} \quad \text{for } i = 0,\ldots,n'_{f1},$$

$$\frac{\partial^i f^{\left(I_{n_f}\right)}}{\partial v_s^i}\Big|_{v_s=0} = 0 \text{ for } i = n'_{f1}+1,\ldots,n_{f1},$$

$$\frac{\partial^i f^{\left(I_{n_f}\right)}}{\partial \omega_s^i}\Big|_{\omega_s=0} = \frac{\partial^i f}{\partial \omega_s^i}\Big|_{\omega_s=0} \text{for } i = 0,\ldots,n'_{f2},$$

$$\frac{\partial^i f^{\left(I_{n_f}\right)}}{\partial \omega_s^i}\Big|_{\omega_s=0} = 0 \text{ for } i = n'_{f2}+1,\ldots,n_{f2}, \tag{45}$$

and where $f = T_{sx}, T_{sy}, M_s$, $n_f = n_{f1}+n_{f2}+1$, $n_{f1} \geq n'_{f1}$ and $n_{f2} \geq n'_{f2}$ and in the case of $n_{f1} = n'_{f1}$ or $n_{f2} = n'_{f2}$ we omit the corresponding index in the parenthesis.

For $n_{T_s} = n_{M_s} = 1$ and $n_{T_{sx}1} = n_{T_{sx}2} = n_{T_{sy}1} = n_{T_{sy}2} = n_{M_s1} = n_{M_s2} = n'_{T_{sx}1} = n'_{T_{sx}2} = n'_{T_{sy}1} = n'_{T_{sy}2} = n'_{M_s1} = n'_{M_s2} = 0$ and using Eqs. (11), (43) and (60)–(62), we get the following coefficients of the approximation

$$a_{T_{sx},0} = c_\varphi,\ a_{T_{sx},1} = -b_{T_{sx}}c^{(x,y)}_{0,1,1},\ a_{T_{sy},0} = s_\varphi,\ a_{T_{sy},1} = b_{T_{sy}}c^{(x,y)}_{1,0,1},$$
$$a_{M_s,0} = s_\varphi c^{(x,y)}_{1,0,0} - c_\varphi c^{(x,y)}_{0,1,0},\ a_{M_s,1} = b_{M_s}c^{(x,y)}_{0,0,-1} \tag{46}$$

and the approximant models take the forms

$$T_{sx}^{(I_{0,0})} = \frac{v_{sx}-b_{T_s}c^{(x,y)}_{0,1,1}\omega_s}{\left(|v_s|^{m_{T_s}}+b_{T_s}^{m_{T_s}}|\omega_s|^{m_{T_s}}\right)^{m_{T_s}^{-1}}},\ T_{sy}^{(I_{0,0})} = \frac{v_{sy}+b_{T_s}c^{(x,y)}_{1,0,1}\omega_s}{\left(|v_s|^{m_{T_s}}+b_{T_s}^{m_{T_s}}|\omega_s|^{m_{T_s}}\right)^{m_{T_s}^{-1}}},$$
$$M_s^{(I_{0,0})} = \frac{b_{M_s}c^{(x,y)}_{0,0,-1}\omega_s - c^{(x,y)}_{0,1,0}v_{sx}+c^{(x,y)}_{1,0,0}v_{sy}}{\left(b_{M_s}^{m_{M_s}}|\omega_s|^{m_{M_s}}+|v_s|^{m_{M_s}}\right)^{m_{M_s}^{-1}}}, \tag{47}$$

where we use relations $v_{sx} = v_s\cos\varphi_s = v_s c_\varphi$ and $v_{sy} = v_s\sin\varphi_s = v_s s_\varphi$.

For $n_{T_s} = n_{M_s} = 3$ and $n_{T_{sx}1} = n_{T_{sx}2} = n_{T_{sy}1} = n_{T_{sy}2} = n_{M_s1} = n_{M_s2} = n'_{T_{sx}1} = n'_{T_{sx}2} = n'_{T_{sy}1} = n'_{T_{sy}2} = n'_{M_s1} = n'_{M_s2} = 1$ and using Eqs. (11), (43) and (60)–(62), we get the following approximant model

$$T_{sx}^{(I_{1,1})} = \frac{v_s^2 v_{sx} - c^{(x,y)}_{1,0,0}v_{sx}v_{sy}\omega_s - c^{(x,y)}_{0,1,0}v_{sy}^2\omega_s + b_{T_s}\left(c^{(x,y)}_{2,0,3}v_{sx}\omega_s^2 + c^{(x,y)}_{1,1,3}v_{sy}\omega_s^2 - c^{(x,y)}_{0,1,1}\omega_s^3\right)}{\left(|v_s|^{3m_{T_s}}+b_{T_s}^{m_{T_s}}|\omega_s|^{3m_{T_s}}\right)^{m_{T_s}^{-1}}},$$
$$T_{sy}^{(I_{1,1})} = \frac{v_s^2 v_{sy} + c^{(x,y)}_{1,0,0}v_{sx}^2\omega_s + c^{(x,y)}_{0,1,0}v_{sx}v_{sy}\omega_s + b_{T_s}\left(c^{(x,y)}_{1,1,3}v_{sx}\omega_s^2 + c^{(x,y)}_{0,2,3}v_{sy}\omega_s^2 + c^{(x,y)}_{1,0,1}\omega_s^3\right)}{\left(|v_s|^{3m_{T_s}}+b_{T_s}^{m_{T_s}}|\omega_s|^{3m_{T_s}}\right)^{m_{T_s}^{-1}}},$$
$$M_s^{(I_{1,1})} = \frac{b_{M_s}c^{(x,y)}_{0,0,-1}\omega_s^3 - c^{(x,y)}_{0,1,0}v_s^2 v_{sx} + c^{(x,y)}_{1,0,0}v_s^2 v_{sy} + c^{(x,y)}_{2,0,0}v_{sx}^2\omega_s + c^{(x,y)}_{0,2,0}v_{sy}^2\omega_s}{\left(b_{M_s}^{m_{M_s}}|\omega_s|^{3m_{M_s}}+|v_s|^{3m_{M_s}}\right)^{m_{M_s}^{-1}}}. \tag{48}$$

In an analogical way higher order approximant models can be constructed. One can note however, that approximation (40) takes the most convenient and regular form for the same highest orders of the fulfilled derivatives for both $v_s = 0$ and $\omega_s = 0$ ($n_{f,1} = n_{f,2}$).

Taking into account the values of integrals $c^{(x,y)}_{i,j,k}$ gathered in Table 1, we get the following forms of models (47) and (48) for elliptic contact

$$T_{sx}^{(I_{0,0})} = \frac{v_{sx}-4b_{T_s}bG(e)I_2 d_s\omega_s}{\left(|v_s|^{m_{T_s}}+b_{T_s}^{m_{T_s}}|\omega_s|^{m_{T_s}}\right)^{m_{T_s}^{-1}}},\ T_{sy}^{(I_{0,0})} = \frac{v_{sy}+4b_{T_s}H(e)I_2 d_c\omega_s}{\left(|v_s|^{m_{T_s}}+b_{T_s}^{m_{T_s}}|\omega_s|^{m_{T_s}}\right)^{m_{T_s}^{-1}}},$$
$$M_s^{(I_{0,0})} = \frac{4b_{M_s}E(e)I_2\omega_s+\pi I_3\left(d_c v_{sy}-bd_s v_{sx}\right)}{\left(b_{M_s}^{m_{M_s}}|\omega_s|^{m_{M_s}}+|v_s|^{m_{M_s}}\right)^{m_{M_s}^{-1}}}, \tag{49}$$

and

$$T_{sx}^{(I_{1,1})} = \frac{v_s^2 v_{sx}+\omega_s\left(b_{T_s}\left(4G(e)I_0 v_{sx}\omega_s - bd_s\left(\pi I_3 v_{sy}^2+4G(e)I_2\omega_s^2\right)\right)-\pi I_3 d_c v_{sx}v_{sy}\right)}{\left(|v_s|^{3m_{T_s}}+b_{T_s}^{m_{T_s}}|\omega_s|^{3m_{T_s}}\right)^{m_{T_s}^{-1}}},$$
$$T_{sy}^{(I_{1,1})} = \frac{v_s^2 v_{sy}+\omega_s\left(b_{T_s}\left(4H(e)I_0 v_{sy}\omega_s + d_c\left(\pi I_3 v_{sx}^2+4H(e)I_2\omega_s^2\right)\right)+\pi bI_3 d_s v_{sx}v_{sy}\right)}{\left(|v_s|^{3m_{T_s}}+b_{T_s}^{m_{T_s}}|\omega_s|^{3m_{T_s}}\right)^{m_{T_s}^{-1}}},$$
$$M_s^{(I_{1,1})} = \frac{4b_{M_s}^{m_f}E(e)I_2\omega_s^3+\pi I_3\left(\left(v_{sx}^2+b^2v_{sy}^2\right)\omega_s+v_s^2\left(d_c v_{sy}-bd_s v_{sx}\right)\right)}{\left(b_{M_s}^{m_{M_s}}|\omega_s|^{3m_{M_s}}+|v_s|^{3m_{M_s}}\right)^{m_{M_s}^{-1}}}. \tag{50}$$

4.2. Piecewise polynomial approximation

For the approximation of exact integral functions (8) we will use the following piecewise polynomial approximation (for the sake of simplicity, we assume here $v_s \geq 0$)

$$f^{(W)}(v_s,\omega_s,\varphi_s) = \begin{cases} \operatorname{sgn}(\omega_s)\sum\limits_{i=0}^{4} a_{f,i}\left(\frac{v_s}{\omega_s}\right)^i & \text{for } v_s \leq |\omega_s|u_{0,f}, \\ \sum\limits_{i=0}^{3} b_{f,i}\left(\frac{\omega_s}{v_s}\right)^i & \text{for } v_s > |\omega_s|u_{0,f}, \end{cases} \tag{51}$$

where $f^{(W)}$ is the approximation of function $f = T_{sx}$, T_{sy}, M_s and $a_{f,i} = a_{f,i}(\varphi_s, \operatorname{sgn}(\omega_s))$, $b_{f,i} = b_{f,i}(\varphi_s, \operatorname{sgn}(\omega_s))$. One can check, that using relations (9), the approximation (51) can be reduced to the function of variables φ_s and θ_s, similarly like the full integral model (10).

The approximations of functions T_{sx} and T_{sy} satisfy up to the first order partial derivatives with respect to variable v_s (for $v_s = 0$) and up to the third order partial derivatives with respect to variable ω_s (for $\omega_s = 0$), of the full integral model. Making use of relations (11) and (60)–(62), one can obtain the following formulae for elliptic contact

$$a_{T_{sx},0} = -c^{(x,y)}_{0,1,1},\quad a_{T_{sx},1} = c^{(x,y)}_{2,0,3}c_\varphi,\quad b_{T_{sx},0} = c_\varphi,$$
$$b_{T_{sx},1} = -c^{(x,y)}_{0,1,0}s_\varphi^2 - c^{(x,y)}_{1,0,0}s_\varphi c_\varphi,$$
$$b_{T_{sx},2} = \frac{1}{2}\left(3\left(c^{(x,y)}_{2,0,0}-c^{(x,y)}_{0,2,0}\right)s_\varphi^2 c_\varphi - c^{(x,y)}_{2,0,0}c_\varphi\right),$$
$$b_{T_{sx},3} = \frac{5}{16}\left(c^{(x,y)}_{0,3,0}-3c^{(x,y)}_{2,1,0}\right)\left(7s_\varphi^4+c_\varphi^4\right)+\frac{5}{2}\left(3c^{(x,y)}_{1,2,0}-c^{(x,y)}_{3,0,0}\right)s_\varphi^3 c_\varphi$$
$$+\frac{1}{8}\left(45c^{(x,y)}_{2,1,0}-11c^{(x,y)}_{0,3,0}\right)s_\varphi^2+3\left(\frac{1}{2}c^{(x,y)}_{3,0,0}-c^{(x,y)}_{2,1,0}\right)s_\varphi c_\varphi$$
$$-\frac{1}{16}\left(5c^{(x,y)}_{3,0,0}+c^{(x,y)}_{2,1,0}\right), \tag{52}$$

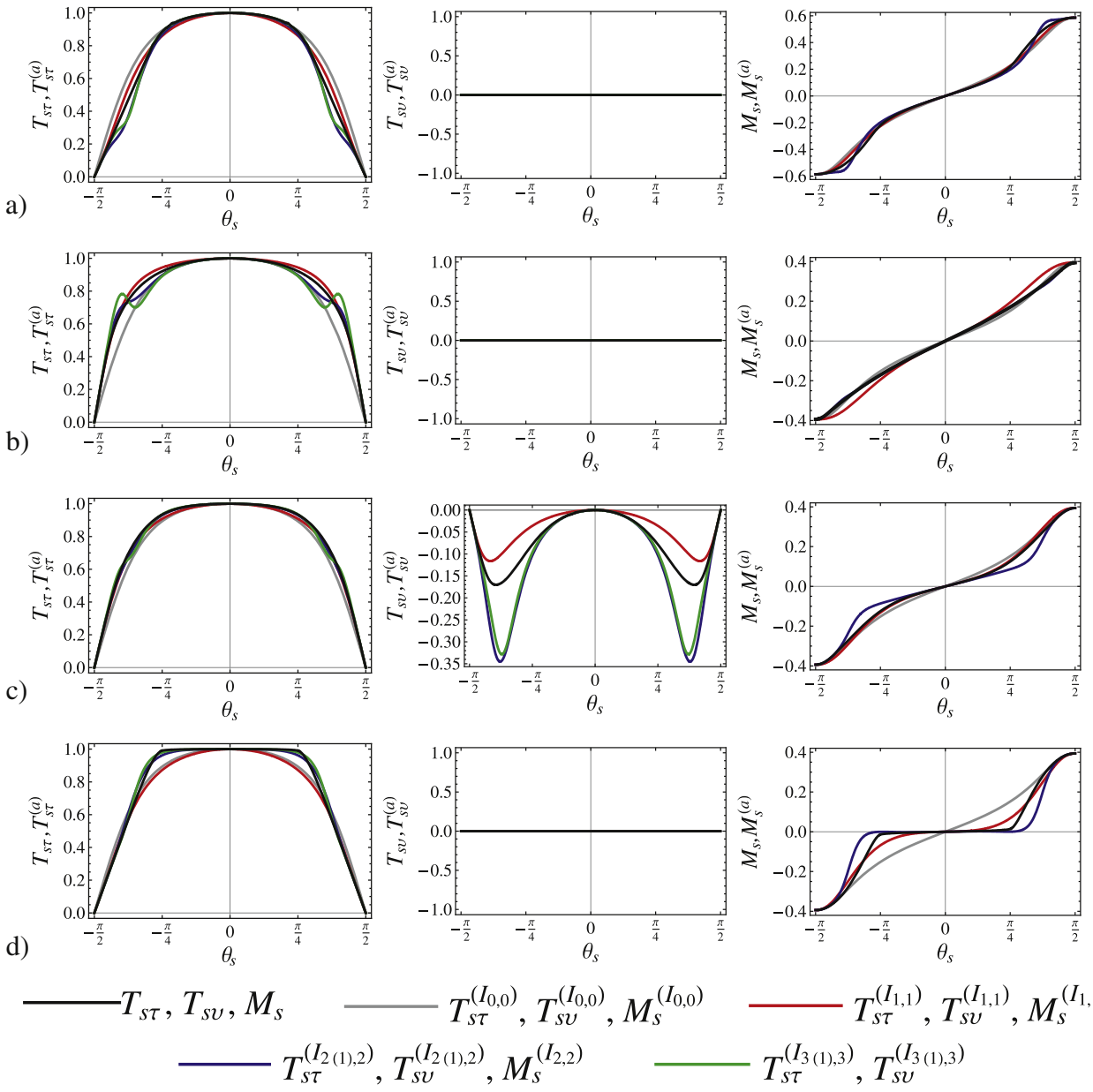

Fig. 8. Comparison of the corresponding components $(T_{s\tau}^{(I_{0,0})}, T_{sv}^{(I_{0,0})}, M_s^{(I_{0,0})}, T_{s\tau}^{(I_{1,1})}, T_{sv}^{(I_{1,1})}, M_s^{(I_{1,1})}, T_{s\tau}^{(I_{2(1),2})}, T_{sv}^{(I_{2(1),2})}, M_s^{(I_{2,2})}, T_{s\tau}^{(I_{3(1),3})}, T_{sv}^{(I_{3(1),3})})$ of selected approximate models (44) and elements $(T_{s\tau}, T_{sv}, M_s)$ of exact integral model (8), for $b = 1$, $\varphi_s = 0$ (a); $b = 0.2$, $\varphi_s = 0$ (b); $b = 0.2$, $\varphi_s = \pi/4$ (c); $b = 0.2$, $\varphi_s = \pi/2$ (d) and for $d = 0$.

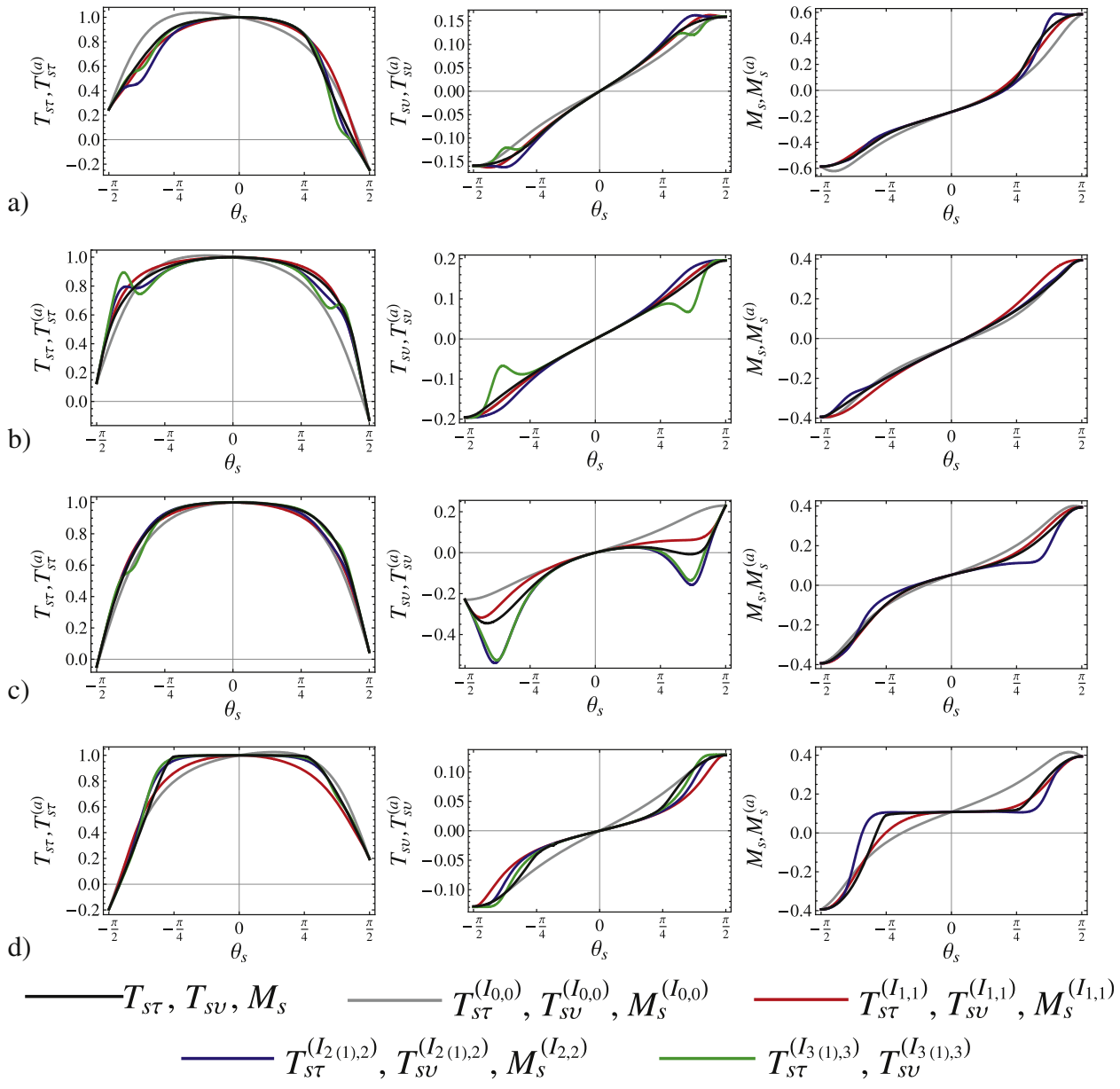

Fig. 9. Comparison of the corresponding components ($T^{(I_{0,0})}_{s\tau}, T^{(I_{0,0})}_{sv}, M^{(I_{0,0})}_s, T^{(I_{1,1})}_{s\tau}, T^{(I_{1,1})}_{sv}, M^{(I_{1,1})}_s, T^{(I_{2(1),2})}_{s\tau}, T^{(I_{2(1),2})}_{sv}, M^{(I_{2,2})}_s, T^{(I_{3(1),3})}_{s\tau}, T^{(I_{3(1),3})}_{sv}$) of selected approximate models (44) and elements ($T_{s\tau}$, T_{sv}, M_s) of exact integral model (8), for $b = 1$, $\varphi_s = 0$ (a); $b = 0.2$, $\varphi_s = 0$ (b); $b = 0.2$, $\varphi_s = \pi/4$ (c); $b = 0.2$, $\varphi_s = \pi/2$ (d) and for $d = 1$ and $\gamma' = 1$.

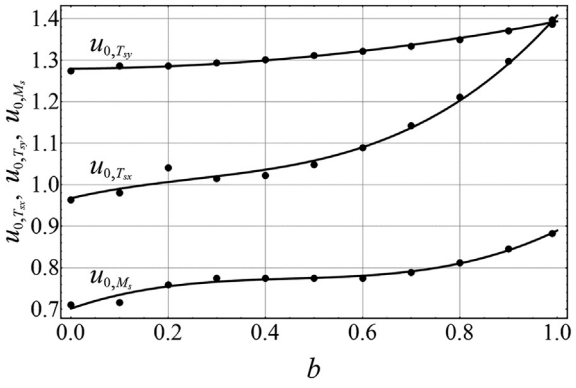

Fig. 10. Results of the optimization of the polynomial joining points for different values of parameter b.

$$
\begin{aligned}
a_{T_{sy},0} &= c^{(x,y)}_{1,0,1}, \quad a_{T_{sy},1} = c^{(x,y)}_{0,2,3} s_\phi, \quad b_{T_{sy},0} = s_\phi,\\
b_{T_{sy},1} &= c^{(x,y)}_{0,1,0} s_\phi c_\phi + c^{(x,y)}_{1,0,0} c^2_\phi,\\
b_{T_{sy},2} &= \frac{1}{2}\left(3\left(c^{(x,y)}_{0,2,0} - c^{(x,y)}_{2,0,0}\right) s_\phi c^2_\phi - c^{(x,y)}_{0,2,0} s_\phi\right),\\
b_{T_{sy},3} &= \frac{5}{16}\left(3c^{(x,y)}_{1,2,0} - c^{(x,y)}_{3,0,0}\right)\left(s^4_\phi + 7c^4_\phi\right) + \frac{5}{2}\left(c^{(x,y)}_{0,3,0} - 3c^{(x,y)}_{2,1,0}\right) s_\phi c^3_\phi\\
&\quad + \frac{1}{8}\left(11c^{(x,y)}_{3,0,0} - 45c^{(x,y)}_{1,2,0}\right) c^2_\phi - 3\left(\frac{1}{2}c^{(x,y)}_{0,3,0} - c^{(x,y)}_{2,1,0}\right) s_\phi c_\phi\\
&\quad + \frac{1}{16}\left(5c^{(x,y)}_{3,0,0} + c^{(x,y)}_{1,2,0}\right),
\end{aligned}
\tag{53}
$$

where coefficients $c^{(x,y)}_{i,j,k}$ are given in Table 1 in Appendix B and where the coefficients equal to zero for elliptic contact area have been removed.

Assuming that friction torque M_s satisfies up to the second order partial derivatives with respect to variable v_s (for $v_s = 0$) and with respect to variable ω_s (for $\omega_s = 0$) of the full integral model, we obtain the following coefficients of approximation

$$
\begin{aligned}
&a_{M_s,0} = c^{(x,y)}_{0,0,-1},\ \ a_{M_s,1} = 0,\ \ a_{M_s,2} = \frac{1}{2}\left(\left(c^{(x,y)}_{0,2,3} - c^{(x,y)}_{2,0,3}\right)c_\varphi^2 - c^{(x,y)}_{0,2,3}\right),\\
&b_{M_s,0} = c^{(x,y)}_{1,0,0}s_\varphi - c^{(x,y)}_{0,1,0}c_\varphi,\ \ b_{M_s,1} = \left(c^{(x,y)}_{2,0,0} - c^{(x,y)}_{0,2,0}\right)c_\varphi^2 - c^{(x,y)}_{0,2,0},\\
&b_{M_s,2} = \frac{3}{2}\left(3c^{(x,y)}_{1,2,0} - c^{(x,y)}_{3,0,0}\right)s_\varphi c_\varphi^2 + \frac{3}{2}\left(3c^{(x,y)}_{2,1,0} - c^{(x,y)}_{0,3,0}\right)c_\varphi^3 - \frac{3}{2}c^{(x,y)}_{1,2,0}s_\varphi\\
&\qquad + 3\left(\frac{1}{2}c^{(x,y)}_{0,3,0} - c^{(x,y)}_{2,1,0}\right)c_\varphi.
\end{aligned}
\tag{54}
$$

The pieces of functions $f^{(W)}$ are joined in points $v_s = |\omega_s|u_{0f}$ $(u_{0f} > 0)$ satisfying the continuity conditions of up to the second order derivatives, giving the following formulae for the rest of the coefficients

$$
\begin{aligned}
a_{f,2} &= -3\mathrm{sgn}(\omega_s)a_{f,1}u_{0f}^{-1} + 6\left(\mathrm{sgn}(\omega_s)b_{f,0} - a_{f,0}\right)u_{0f}^{-2}\\
&\quad + 10b_{f,1}u_{0f}^{-3} + 15\mathrm{sgn}(\omega_s)b_{f,2}u_{0f}^{-4} + 21b_{f,3}u_{0f}^{-5},\\
a_{f,3} &= 3a_{f,1}u_{0f}^{-2} + 8\left(\mathrm{sgn}(\omega_s)a_{f,0} - b_{f,0}\right)u_{0f}^{-3} - 15\mathrm{sgn}(\omega_s)b_{f,1}u_{0f}^{-4}\\
&\quad + 24b_{f,2}u_{0f}^{-5} - 35\mathrm{sgn}(\omega_s)b_{f,3}u_{0f}^{-6},\\
a_{f,4} &= -\mathrm{sgn}(\omega_s)a_{f,1}u_{0f}^{-3} + 3\left(\mathrm{sgn}(\omega_s)b_{f,0} - a_{f,0}\right)u_{0f}^{-4} + 6b_{f,1}u_{0f}^{-5}\\
&\quad + 10\mathrm{sgn}(\omega_s)b_{f,2}u_{0f}^{-6} + 15b_{f,3}u_{0f}^{-7},
\end{aligned}
\tag{55}
$$

for the approximate friction force models $f = T_{sx}, T_{sy}$. In the case of the friction torque model we have the following expressions

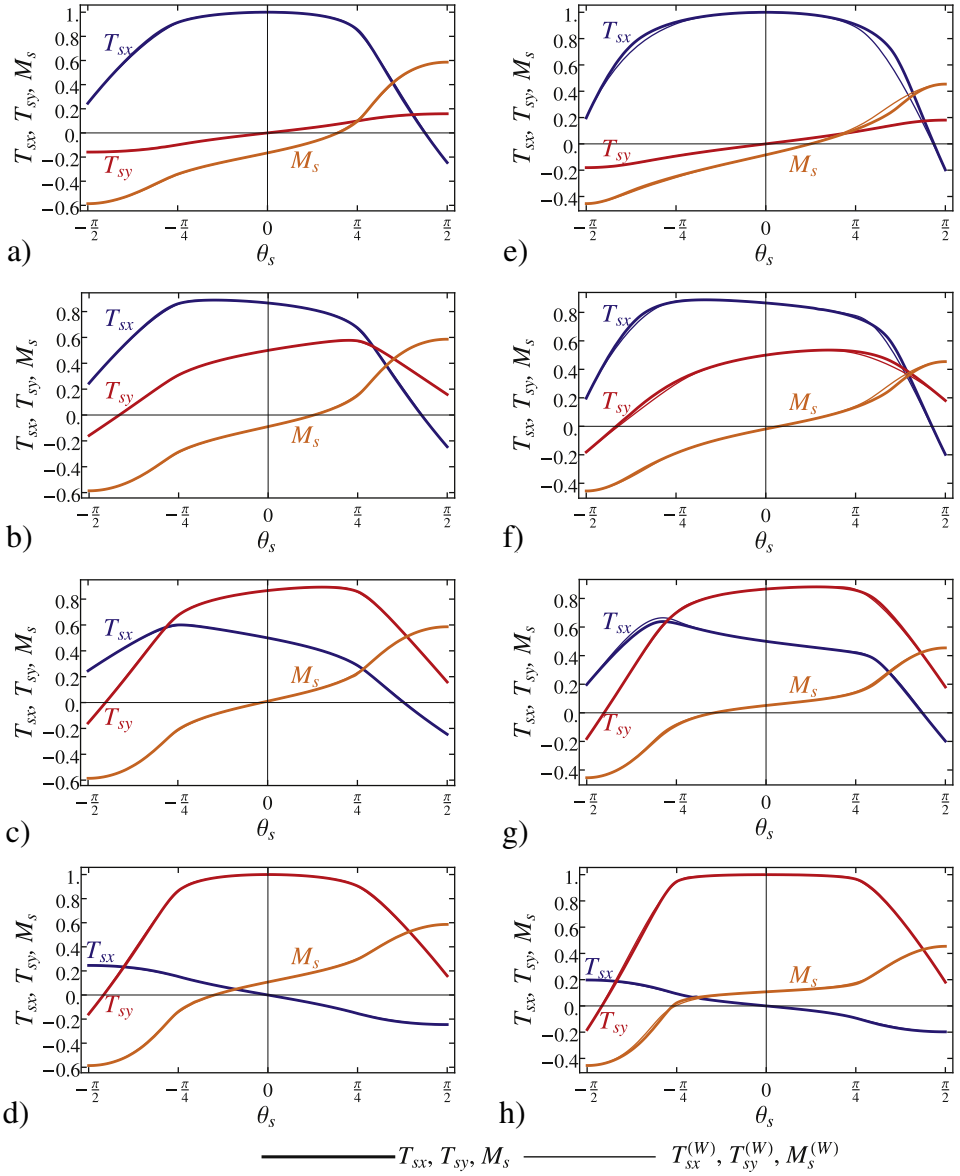

Fig. 11. Comparison of the corresponding components $(T_{sx}^{(W)}, T_{sy}^{(W)}, M_s^{(W)})$ of approximate model (51) and elements (T_{sx}, T_{sy}, M_s) of exact integral model (8), for $b = 1$ (a–d), $b = 0.5$ (e–h), $\varphi_s = 0$ (a, e), $\varphi_s = \pi/6$ (b, f), $\varphi_s = \pi/3$ (c, g) and $\varphi_s = \pi/2$ (d, h). The values of the remaining parameters: $d = 1$ and $\gamma' = 1$.

$$
\begin{aligned}
a_{M_s,3} &= -\frac{5}{3}\operatorname{sgn}(\omega_s)a_{M_s,2}u_{0,M_s}^{-1} - 2a_{M_s,1}u_{0,M_s}^{-2} + 2\left(b_{M_s,0} - \operatorname{sgn}(\omega_s)a_{M_s,0}\right)u_{0,M_s}^{-3} + \frac{5}{3}\operatorname{sgn}(\omega_s)b_{M_s,1}u_{0,M_s}^{-4} + b_{M_s,2}u_{0,M_s}^{-5},\\
a_{M_s,4} &= \frac{1}{7}\left(5a_{M_s,2}u_{0,M_s}^{-2} + 8\operatorname{sgn}(\omega_s)a_{M_s,1}u_{0,M_s}^{-3} + 9\left(a_{M_s,0} - \operatorname{sgn}(\omega_s)b_{M_s,0}\right)u_{0,M_s}^{-4} + -8b_{M_s,1}u_{0,M_s}^{-5} - 5\operatorname{sgn}(\omega_s)b_{M_s,2}u_{0,M_s}^{-6}\right),\\
b_{M_s,3} &= \frac{1}{21}\left(-15\operatorname{sgn}(\omega_s)b_{M_s,2}u_{0,M_s} - 10b_{M_s,1}u_{0,M_s}^{2} + 6\left(a_{M_s,0} - \operatorname{sgn}(\omega_s)b_{M_s,0}\right)u_{0,M_s}^{3} + 3\operatorname{sgn}(\omega_s)a_{M_s,1}u_{0,M_s}^{4} + a_{M_s,2}u_{0,M_s}^{5}\right).
\end{aligned}
\tag{56}
$$

The additional three parameters $u_{0,T_{sx}}$, $u_{0,T_{sy}}$ and u_{0,M_s} (defining the points of the polynomial joining) are independent from the corresponding derivatives of the integral model of friction and can be chosen arbitrarily.

4.3. Examples for Hertz nominal stress distribution

In this section we present a comparison of some above introduced approximate models with the full integral model of friction (8) for the Hertz case of nominal stress distribution, that is for $\sigma_0'(\rho') = 3/2\pi\sqrt{1-\rho'^2}$ (cf. Sect. 3). In these examples we assume the coefficients $c_{i,j,k}^{(x,y)}$ of the approximate models according to Table 1 in Appendix B, for the following parameters

$$
I_0 = \tfrac{3}{8},\quad I_2 = \tfrac{3}{32},\quad I_3 = \tfrac{1}{5\pi},\quad I_5 = \tfrac{4}{35\pi},
\tag{57}
$$

for both exact and approximate models. The last formulae (note that relation $I_{i+1} \le I_i$ holds for any non-negative integer i) are obtained according to definition (23) for $\sigma_0'(\rho') = 3/2\pi\sqrt{1-\rho'^2}$.

Figs. 8 and 9 exhibit a comparison of the components $(T_{s\tau}^{(I_{0,0})}, T_{sv}^{(I_{0,0})}, M_s^{(I_{0,0})}, T_{s\tau}^{(I_{1,1})}, T_{sv}^{(I_{1,1})}, M_s^{(I_{1,1})}, T_{s\tau}^{(I_{2(1),2})}, T_{sv}^{(I_{2(1),2})}, M_s^{(I_{2,2})}, T_{s\tau}^{(I_{3(1),3})}, T_{sv}^{(I_{3(1),3})})$ of selected approximant models (44) with the corresponding

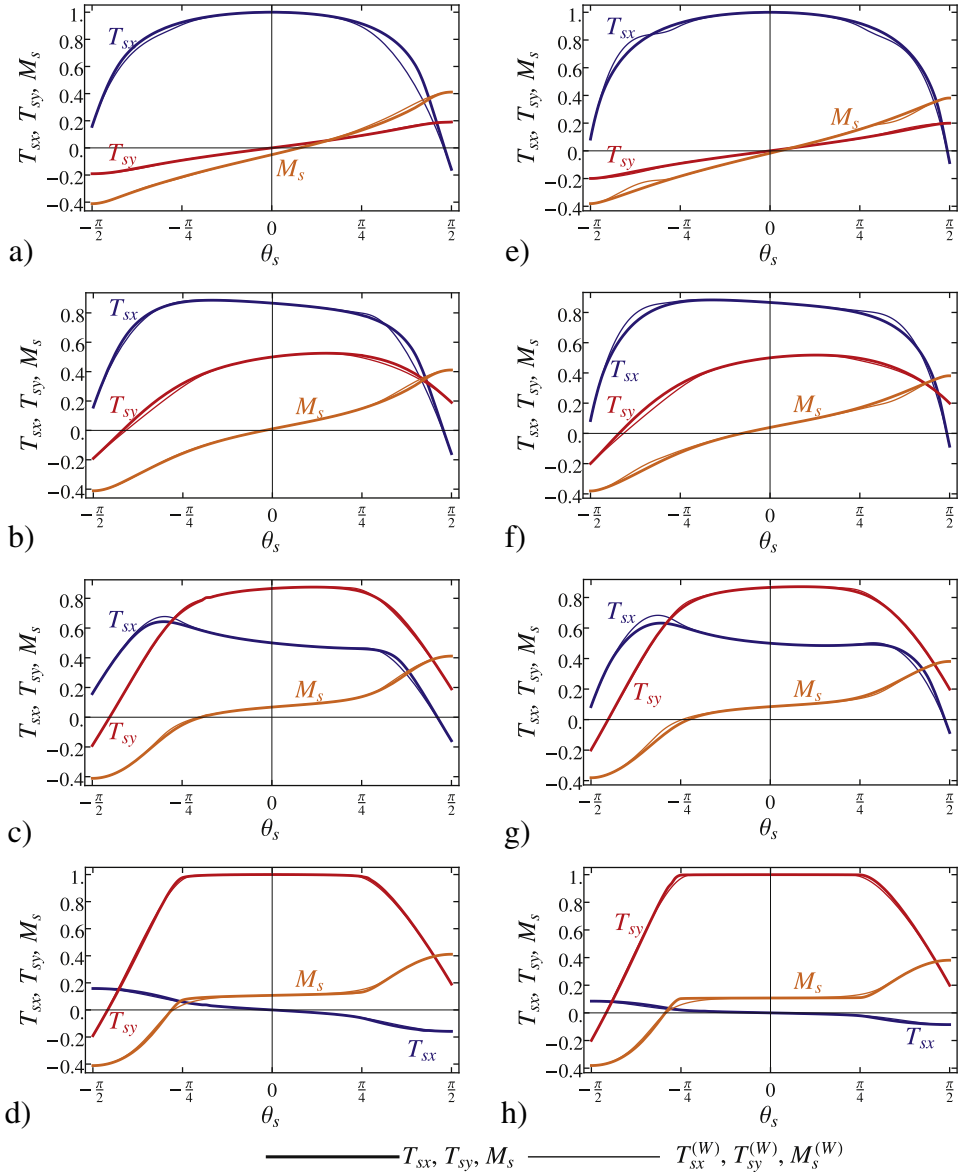

Fig. 12. Comparison of the corresponding components $(T_{sx}^{(W)}, T_{sy}^{(W)}, M_s^{(W)})$ of approximate model (51) and elements (T_{sx}, T_{sy}, M_s) of exact integral model (8), for $b = 0.3$ (a–d), $b = 0.1$ (e–h), $\varphi_s = 0$ (a, e), $\varphi_s = \pi/6$ (b, f), $\varphi_s = \pi/3$ (c, g) and $\varphi_s = \pi/2$ (d, h). The values of the remaining parameters: $d = 1$ and $\gamma' = 1$.

components ($T_{s\tau}$, T_{sv}, M_s) of the exact integral model (8) obtained numerically. Even though the approximants have been constructed in the coordinate system Axy, the results are presented in the coordinate system $A\tau v$. The Figures exhibit plots for the range $\theta_s \in \langle -\pi/2, \pi/2\rangle$ only, since all the presented functions $f(\theta_s)$ possess the property $f(\theta_s+\pi) = -f(\theta_s)$. The coefficients m_{T_s}, m_{M_s}, b_{T_s} and b_{M_s} have been determined by the use of optimization of the corresponding approximant and integral model matching for full ranges of variation of the corresponding parameters and variables: $0 < b \le 1$, $0 \le d \le 1$, $0 \le \gamma \le 2\pi$, $-\pi/2 \le \theta_s \le \pi/2$ and $0 \le \varphi_s \le 2\pi$. Fig. 8 presents results for the case without rolling resistance ($d = 0$), while Fig. 9 exhibits results for rolling resistance with $d = 1$. One can note that the higher degree of the approximant do not always leads to better results. In the presented examples the best fitting is obtained for the approximations $I_{1,1}$.

For $f^{(W)}$ approximations (cf. Sect. 4.2), parameters $u_{0,T_{sx}}$, $u_{0,T_{sy}}$ and u_{0,M_s} (defining the points of polynomial joining) have been selected for 11 different values of parameter b basing on the optimization procedure. The sum of square deviations of the approximate model from the exact integral model for different values of the remaining parameters (φ_s, θ_s, d and γ') has been chosen as a criterion being minimized. The optimization results are shown in Fig. 10 together with the plots of polynomials fitted to the obtained results and having the following forms

$$\begin{aligned} u_{0,T_{sx}}(b) &= 0.967 + 0.276b - 0.542b^2 + 0.706b^3, \\ u_{0,T_{sy}}(b) &= 1.280 + 0.007b + 0.106b^2, \\ u_{0,M_s}(b) &= 0.702 + 0.407b - 0.819b^2 + 0.600b^3. \end{aligned} \tag{58}$$

Figs. 11 and 12 illustrate a comparison of the corresponding components of approximate, piecewise polynomial model ($T_{sx}^{(W)}$, $T_{sy}^{(W)}$, $M_s^{(W)}$) and exact integral model (T_{sx}, T_{sy}, M_s). Fig. 11 exhibits results for the circular ($b = 1$) and elliptic contact area of moderate eccentricity ($b = 0.5$). Fig. 12 shows results for higher eccentricities of the contact ($b = 0.3$ and $b = 0.1$). For each eccentricity value the four plots for different angles $\varphi_s = i\pi/6$ ($i = 0, 1, 2, 3$) are performed, while the other parameters are $d = 1$ and $\gamma' = 1$. In Fig. 11 one can observe, that for the circular contact patch the approximate model gives practically exact results. In that case the lower order approximation would be probably sufficient. The elaborated piecewise polynomial model gives, however, very good results for $b = 0.5$ as well and quite good results for more slender ($b = 0.3$ and $b = 0.1$ in Fig. 12). The highest approximation errors are observed for $b = 0.3$ (in some cases the absolute error of the approximation of non-dimensional component T_{sx} reaches the value of about 0.15, that is about 15% of the maximal magnitude). Let us note that the approximate model exhibits the highest errors for the T_{sx} component (along the longer axis of the contact), whereas in the case of the second component of the friction force T_{sy} and friction torque M_s the approximation gives almost perfect results.

5. Concluding remarks

The work aims at developing the approximate models of coupled friction and rolling resistance in the case of elliptic contact. The resulting model is sufficient for fast numerical simulations of rigid bodies with frictional contacts, since it allows to avoid using numerical methods basing on space discretization.

The rolling friction model is built as a resistance against movement of the deformed zone (contour friction) which is related to the fact that stresses for growing strains are greater than stresses for the same but diminishing strains (elastic hysteresis phenomenon). In the elaborated rolling resistance model some simplifications were assumed. In the general case, rotational motion of the deformation zone (not taken into account) can also have some influence on the contact stress distribution and rolling resistance.

The corresponding approximate models can easily be developed for other shapes of the contact area and normal stress distribution, since in Sect. 2 some expressions being the base of approximation are given for the general case of contact.

Acknowledgements

This paper was financially supported by the National Science Centre of Poland under the grant MAESTRO 2, No. 2012/04/A/ST8/00738, for years 2013–2016.

Appendix A. Some properties of the integral model of friction

In Sect. 2, the values of the exact integral model of friction (8), for $v_s = 0$ (assuming $\omega_s \neq 0$) and for $\omega_s = 0$ (assuming $v_s \neq 0$), are given. It is also possible to derive further properties of the model, i.e. the corresponding higher order partial derivatives of the functions (8). For example, the partial derivatives of the first order have the following form

$$\begin{aligned} \left.\frac{\partial T_{sx}}{\partial v_s}\right|_{v_s=0} &= \left(c_{1,1,3}^{(x,y)} s_\varphi + c_{2,0,3}^{(x,y)} c_\varphi\right) \frac{1}{|\omega_s|}, \\ \left.\frac{T_{sx}}{\partial \omega_s}\right|_{\omega_s=0} &= -\left(c_{0,1,0}^{(x,y)} s_\varphi^2 + c_{1,0,0}^{(x,y)} s_\varphi c_\varphi\right) \frac{1}{|v_s|}, \\ \left.\frac{\partial T_{sy}}{\partial v_s}\right|_{v_s=0} &= \left(c_{0,2,3}^{(x,y)} s_\varphi + c_{1,1,3}^{(x,y)} c_\varphi\right) \frac{1}{|\omega_s|}, \\ \left.\frac{\partial T_{sy}}{\partial \omega_s}\right|_{\omega_s=0} &= \left(c_{0,1,0}^{(x,y)} s_\varphi c_\varphi + c_{1,0,0}^{(x,y)} c_\varphi^2\right) \frac{1}{|v_s|}, \qquad \left.\frac{\partial M_s}{\partial v_s}\right|_{v_s=0} = 0, \\ \left.\frac{\partial M_s}{\partial \omega_s}\right|_{\omega_s=0} &= \left(\left(c_{0,2,0}^{(x,y)} - c_{2,0,0}^{(x,y)}\right) s_\varphi^2 + 2c_{1,1,0}^{(x,y)} s_\varphi c_\varphi + c_{2,0,0}^{(x,y)}\right) \frac{1}{|v_s|}, \end{aligned} \tag{59}$$

and partial derivatives of the second order read

$$\begin{aligned} \left.\frac{\partial^2 T_{sx}}{\partial v_s^2}\right|_{v_s=0} &= \left(\left(c_{0,3,5}^{(x,y)} - 5c_{2,1,5}^{(x,y)}\right) s_\varphi^2 + 2\left(2c_{1,2,5}^{(x,y)} - c_{3,0,5}^{(x,y)}\right) s_\varphi c_\varphi + 3c_{2,1,5}^{(x,y)}\right) \frac{1}{\omega_s|\omega_s|}, \\ \left.\frac{\partial^2 T_{sx}}{\partial \omega_s^2}\right|_{\omega_s=0} &= \left(6c_{1,1,0}^{(x,y)} s_\varphi^3 + 3\left(c_{2,0,0}^{(x,y)} - c_{0,2,0}^{(x,y)}\right) s_\varphi^2 c_\varphi - 4c_{1,1,0}^{(x,y)} s_\varphi - c_{2,0,0}^{(x,y)} c_\varphi\right) \frac{1}{v_s|v_s|}, \\ \left.\frac{\partial^2 T_{sy}}{\partial v_s^2}\right|_{v_s=0} &= \left(2\left(c_{0,3,5}^{(x,y)} - 2c_{2,1,5}^{(x,y)}\right) s_\varphi c_\varphi + \left(5c_{1,2,5}^{(x,y)} - c_{3,0,5}^{(x,y)}\right) c_\varphi^2 - 3c_{1,2,5}^{(x,y)}\right) \frac{1}{\omega_s|\omega_s|}, \\ \left.\frac{\partial^2 T_{sy}}{\partial \omega_s^2}\right|_{\omega_s=0} &= \left(3\left(c_{0,2,0}^{(x,y)} - c_{2,0,0}^{(x,y)}\right) s_\varphi c_\varphi^2 + 6c_{1,1,0}^{(x,y)} c_\varphi^3 - c_{0,2,0}^{(x,y)} s_\varphi - 4c_{1,1,0}^{(x,y)} c_\varphi\right) \frac{1}{v_s|v_s|}, \\ \left.\frac{\partial^2 M_s}{\partial v_s^2}\right|_{v_s=0} &= -\left(2c_{1,1,3}^{(x,y)} s_\varphi c_\varphi - \left(c_{0,2,3}^{(x,y)} - c_{2,0,3}^{(x,y)}\right) c_\varphi^2 + c_{0,2,3}^{(x,y)}\right) \frac{1}{\omega_s|\omega_s|}, \\ \left.\frac{\partial^2 M_s}{\partial \omega_s^2}\right|_{\omega_s=0} &= 3\left(\left(3c_{1,2,0}^{(x,y)} - c_{3,0,0}^{(x,y)}\right) s_\varphi c_\varphi^2 + \left(3c_{2,1,0}^{(x,y)} - c_{0,3,0}^{(x,y)}\right) c_\varphi^3 - c_{1,2,0}^{(x,y)} s_\varphi + \left(c_{0,3,0}^{(x,y)} - 2c_{2,1,0}^{(x,y)}\right) c_\varphi\right) \frac{1}{v_s|v_s|} \end{aligned} \tag{60}$$

while the derivatives of the third order equal

$$\begin{aligned}
\frac{\partial^3 T_{sx}}{\partial v_s^3}\Big|_{v_s=0} &= 3\Big(\Big(11c_{3,1,7}^{(x,y)}-9c_{1,3,7}^{(x,y)}\Big)s_\phi^3+\Big(3c_{4,0,7}^{(x,y)}-15c_{2,2,7}^{(x,y)}+2c_{0,4,7}^{(x,y)}\Big)s_\phi^2c_\phi+\Big(6c_{1,3,7}^{(x,y)}-9c_{3,1,7}^{(x,y)}\Big)s_\phi+\Big(4c_{2,2,7}^{(x,y)}-c_{4,0,7}^{(x,y)}\Big)c_\phi\Big)\frac{1}{\omega_s^2|\omega_s|},\\
\frac{\partial^3 T_{sx}}{\partial \omega_s^3}\Big|_{\omega_s=0} &= 3\Big(\Big(5c_{0,3,0}^{(x,y)}-15c_{2,1,0}^{(x,y)}\Big)s_\phi^4+\Big(15c_{1,2,0}^{(x,y)}-5c_{3,0,0}^{(x,y)}\Big)s_\phi^3c_\phi+\Big(15c_{2,1,0}^{(x,y)}-4c_{0,3,0}^{(x,y)}\Big)s_\phi^2+\Big(3c_{3,0,0}^{(x,y)}-6c_{1,2,0}^{(x,y)}\Big)s_\phi c_\phi-2c_{2,1,0}^{(x,y)}\Big)\frac{1}{v_s^2|v_s|},\\
\frac{\partial^3 T_{sy}}{\partial v_s^3}\Big|_{v_s=0} &= 3\Big(\Big(3c_{0,4,7}^{(x,y)}-15c_{2,2,7}^{(x,y)}+2c_{4,0,7}^{(x,y)}\Big)s_\phi c_\phi^2+\Big(11c_{1,3,7}^{(x,y)}-9c_{3,1,7}^{(x,y)}\Big)c_\phi^3+\Big(4c_{2,2,7}^{(x,y)}-c_{0,4,7}^{(x,y)}\Big)s_\phi+\Big(6c_{3,1,7}^{(x,y)}-9c_{1,3,7}^{(x,y)}\Big)c_\phi\Big)\frac{1}{\omega_s^2|\omega_s|},\\
\frac{\partial^3 T_{sy}}{\partial \omega_s^3}\Big|_{\omega_s=0} &= 3\Big(\Big(5c_{0,3,0}^{(x,y)}-15c_{2,1,0}^{(x,y)}\Big)s_\phi c_\phi^3+\Big(15c_{1,2,0}^{(x,y)}-5c_{3,0,0}^{(x,y)}\Big)c_\phi^4+\Big(6c_{2,1,0}^{(x,y)}-3c_{0,3,0}^{(x,y)}\Big)s_\phi c_\phi+\Big(4c_{3,0,0}^{(x,y)}-15c_{1,2,0}^{(x,y)}\Big)c_\phi^2+2c_{1,2,0}^{(x,y)}\Big)\frac{1}{v_s^2|v_s|},\\
\frac{\partial^3 M_s}{\partial v_s^3}\Big|_{v_s=0} &= 3\Big(\Big(2c_{3,0,5}^{(x,y)}-6c_{1,2,5}^{(x,y)}\Big)s_\phi c_\phi^2+\Big(2c_{0,3,5}^{(x,y)}-6c_{2,1,5}^{(x,y)}\Big)c_\phi^3+2c_{1,2,5}^{(x,y)}s_\phi+\Big(4c_{2,1,5}^{(x,y)}-2c_{0,3,5}^{(x,y)}\Big)c_\phi\Big)\frac{1}{\omega_s^2|\omega_s|},\\
\frac{\partial^3 M_s}{\partial \omega_s^3}\Big|_{\omega_s=0} &= 3\Big(5\Big(6c_{2,2,0}^{(x,y)}-c_{0,4,0}^{(x,y)}-c_{4,0,0}^{(x,y)}\Big)s_\phi^4+20\Big(c_{3,1,0}^{(x,y)}-c_{1,3,0}^{(x,y)}\Big)s_\phi^3c_\phi+\Big(6c_{4,0,0}^{(x,y)}+4c_{0,4,0}^{(x,y)}-30c_{2,2,0}^{(x,y)}\Big)s_\phi^2+\Big(8c_{1,3,0}^{(x,y)}-12c_{3,1,0}^{(x,y)}\Big)s_\phi c_\phi\\
&\quad +4c_{2,2,0}^{(x,y)}-c_{4,0,0}^{(x,y)}\Big)\frac{1}{v_s^2|v_s|}
\end{aligned}\tag{61}$$

where s_φ, c_φ and $c_{i,j,k}^{(\zeta,\eta)}$ are defined by Eqs. (12) and (13).

Appendix B. The characteristic integrals of the friction model for elliptic contact area

Table 1 shows the setting-up of values of the most important integrals $c_{i,j,k}^{(x,y)}$ occurring in expressions (11) and (59)–(61), with the assumption of a normal stress distribution model defined by Eq. (16). In order to shorten the notation, the following functions have been introduced

$$G(e)=(K(e)-E(e))e^{-2},\ H(e)=\Big(E(e)+\Big(e^2-1\Big)K(e)\Big)e^{-2},\tag{62}$$

where $K(e)$ and $E(e)$ are the complete elliptic integrals of the first and second kind, respectively

$$K(e)=\int_0^{\pi/2}\frac{d\phi}{\sqrt{1-e^2\sin^2\phi}},\ E(e)=\int_0^{\pi/2}\sqrt{1-e^2\sin^2\phi}\,\mathrm{d}\phi\tag{63}$$

and where e stands for eccentricity of the contact area ($0\le e=\sqrt{1-b^2}<1$).

Beside the values of integrals $c_{i,j,k}^{(x,y)}$ for the general case of elliptic contact, Table 1 contains also limits of the integrals for $b\to1$ (circular contact) and for $b\to0$ (line contact as a degenerated elliptic one). In the second case one can see that some of the integrals (e.g. $c_{2,0,3}^{(x,y)}$) tend to infinity and make impossible to use certain approximate models based on derivatives (11) and (59)–(61). One can use the approximations omitting certain properties of the integral model (these approximations may occur improper) or use approximate models for elliptic contact of b parameter very close to zero.

Table 1
Setting-up of part of integrals occurring in expressions (11) and (59)–(61) for stress $\sigma(x,y)$ distribution model according to (16).

Notation of the integral according to (13)	The full form of integral in the *Axy* coordinate system	Value of the integral	Limit $\lim_{b\to1} c_{i,j,k}^{(x,y)}$	Limit $\lim_{b\to0} c_{i,j,k}^{(x,y)}$
$c_{1,0,0}^{(x,y)}$	$\iint_F x\sigma(x,y)\mathrm{d}x\mathrm{d}y$	$\pi I_3 d_c$	$\pi I_3 d_c$	$\pi I_3 d_c$
$c_{0,1,0}^{(x,y)}$	$\iint_F y\sigma(x,y)\mathrm{d}x\mathrm{d}y$	$\pi b I_3 d_s$	$\pi I_3 d_s$	0

Table 1 (*continued*)

Notation of the integral according to (13)	The full form of integral in the *Axy* coordinate system	Value of the integral	Limit $\lim_{b\to1} c_{i,j,k}^{(x,y)}$	Limit $\lim_{b\to0} c_{i,j,k}^{(x,y)}$
$c_{0,1,1}^{(x,y)}$	$\iint_F \frac{y\sigma(x,y)}{\sqrt{x^2+y^2}}\mathrm{d}x\mathrm{d}y$	$4bG(e)I_2d_s$	$\pi I_2 d_s$	0
$c_{1,0,1}^{(x,y)}$	$\iint_F \frac{x\sigma(x,y)}{\sqrt{x^2+y^2}}\mathrm{d}x\mathrm{d}y$	$4H(e)I_2d_c$	$\pi I_2 d_c$	$4I_2d_c$
$c_{2,0,3}^{(x,y)}$	$\iint_F \frac{x^2\sigma(x,y)}{(x^2+y^2)^{3/2}}\mathrm{d}x\mathrm{d}y$	$4G(e)I_0$	πI_0	∞
$c_{2,0,0}^{(x,y)}$	$\iint_F x^2\sigma(x,y)\mathrm{d}x\mathrm{d}y$	πI_3	πI_3	πI_3
$c_{0,2,0}^{(x,y)}$	$\iint_F y^2\sigma(x,y)\mathrm{d}x\mathrm{d}y$	$\pi b^2 I_3$	πI_3	0
$c_{0,0,-1}^{(x,y)}$	$\iint_F \sqrt{x^2+y^2}\sigma(x,y)\mathrm{d}x\mathrm{d}y$	$4E(e)I_2$	$2\pi I_2$	$4I_2$
$c_{0,2,3}^{(x,y)}$	$\iint_F \frac{y^2\sigma(x,y)}{(x^2+y^2)^{3/2}}\mathrm{d}x\mathrm{d}y$	$4H(e)I_0$	πI_0	$4I_0$
$c_{1,1,3}^{(x,y)}$	$\iint_F \frac{xy\sigma(x,y)}{(x^2+y^2)^{3/2}}\mathrm{d}x\mathrm{d}y$	0	0	0
$c_{1,1,0}^{(x,y)}$	$\iint_F xy\sigma(x,y)\mathrm{d}x\mathrm{d}y$	0	0	0
$c_{1,2,0}^{(x,y)}$	$\iint_F xy^2\sigma(x,y)\mathrm{d}x\mathrm{d}y$	$\frac{\pi}{4}b^2I_5d_c$	$\frac{\pi}{4}I_5d_c$	0
$c_{2,1,0}^{(x,y)}$	$\iint_F x^2y\sigma(x,y)\mathrm{d}x\mathrm{d}y$	$\frac{\pi}{4}bI_5d_s$	$\frac{\pi}{4}I_5d_s$	0
$c_{3,0,0}^{(x,y)}$	$\iint_F x^3\sigma(x,y)\mathrm{d}x\mathrm{d}y$	$\frac{3\pi}{4}I_5d_c$	$\frac{3\pi}{4}I_5d_c$	$\frac{3\pi}{4}I_5d_c$
$c_{0,3,0}^{(x,y)}$	$\iint_F y^3\sigma(x,y)\mathrm{d}x\mathrm{d}y$	$\frac{3\pi}{4}b^3I_5d_s$	$\frac{3\pi}{4}I_5d_s$	0

Appendix C. Approximation of the elliptic integrals

For numerical approximation of functions $K(e)$ and $E(e)$ for $0\le e<1$ one can use the following series (Milne-Thomson, 1972; Whittaker and Watson, 2002; Kosenko and Aleksandrov, 2009)

$$\begin{aligned}
K_{n_q,n_K} &= \frac{\pi}{2}\left(1+2\sum_{n=1}^{n_K}q_{n_q}^{n^2}\right)^2,\\
E_{n_q,n_K,n_E} &= \frac{2-e^2}{3}K_{n_q,n_K}+\frac{\pi^2}{K_{n_q,n_K}}\left(\frac{1}{12}-2\sum_{n=1}^{n_E}\frac{q_{n_q}^{2n}}{\left(1-q_{n_q}^{2n}\right)^2}\right),\\
\text{where}\quad q_{n_q} &= \sum_{n=1}^{n_q}a_n\varepsilon^{4(n-1)+1},
\end{aligned}\tag{64}$$

and where a_n is the n-th element of the series 1, 2, 15, 150, 1707, …, whereas the $\varepsilon(e)$ function is defined as follows

$$\varepsilon=\frac{1}{2}\cdot\frac{1-\left(1-e^2\right)^{1/4}}{1+\left(1-e^2\right)^{1/4}}.\tag{65}$$

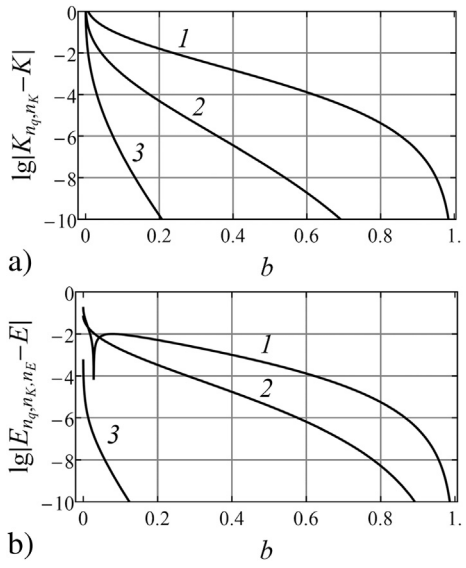

Fig. 13. Errors of approximations ((64) and (65)) of elliptic integrals $K(e)$ and $E(e)$ (where $b = \sqrt{1-e^2}$), for the following parameters: a) $n_q = 1$, $n_K = 1$ (1); $n_q = 2$, $n_K = 2$ (2); $n_q = 5$, $n_K = 4$ (3); b) $n_q = 1$, $n_K = 1$, $n_E = 1$ (1); $n_q = 2$, $n_K = 2$, $n_E = 2$ (2); $n_q = 5$, $n_K = 4$, $n_E = 8$ (3).

For $n_q, n_K, n_E \to \infty$ we have $K_{n_q,n_K}(e) \to K(e)$ and $E_{n_q,n_K,n_E}(e) \to E(e)$. Fig. 13 presents errors of approximations of functions K and E as the functions of $b = \sqrt{1-e^2}$ argument for different values of parameters n_q, n_K and n_E. It comes out that for sufficiently large parameter b and taking into account uncertainties related to the real contact pressure distribution as well as inaccuracies of the approximate models presented in the next subsection, approximation ((64) and (65)) can be sufficient even for $n_q = 1$, $n_K = 1$ and $n_E = 1$ (but it depends on the kind of application of the corresponding approximation).

References

Contensou, P., 1962. Couplage entre frottement de glissement et de pivotement dans la téorie de la toupe. In: Kreiselprobleme Gyrodynamics: IUTAM Symp. Calerina, pp. 201–216.

Greenwood, J.A., Minshall, H., Tabor, D., 1961. Hysteresis losses in rolling and sliding friction. Proceedings of the Royal Society of London. Series A 259, 480–507.

Johnson, K.L., 1985. Contact Mechanics. Cambridge University Press, Cambridge.

Kireenkov, A.A., 2005. About the motion of the symmetric rigid solid along the plane. In: 8th Conference on DSTA, Łódź, pp. 95–102.

Kireenkov, A.A., 2008. Combined model of sliding and rolling friction in dynamics of bodies on a rough plane. Mechanics of Solids 43 (3), 412–425.

Kosenko, I., Aleksandrov, E., 2009. Implementation of the Contensou-Erisman model of friction in frame of the Hertz contact problem on Modelica. In: 7th Modelica Conference, Como, Italy, pp. 288–298.

Leine, R.I., 2009. Measurements of the finite-time singularity of the Euler disk. In: 7th EUROMECH Solid Mechanical Conference, Lisbon, Portugal.

Leine, R.I., Glocker, Ch, 2003. A set-valued force law for spatial Coulomb-Contensou friction. European Journal of Mechanics A/Solids 22 (2), 193–216.

Leine, R.I., Le Saux, C., Glocker, Ch, 2005. Friction models for the rolling disk. In: Proceedings of the 5th EUROMECH Nonlinear Dynamics Conference (ENOC 2005), Eindhoven, The Netherlands.

Leine, R.I., Van De Wouw, N., 2008. Stability and Convergence of Mechanical Systems with Unilateral Constraints. Springer-Verlag, Berlin, New York.

Milne-Thomson, L.M., 1972. Elliptic integrals. In: Abramowitz, M., Stegun, I.A. (Eds.), Hand-book of Mathematical Functions: With Formulas, Graphs, and Mathematical Tables. Dover Publications Inc., New York.

Svedenius, J., 2003. Tire Models for Use in Braking Application (Licentiate thesis). Lund University.

Tabor, D., 1955. The mechanism of rolling friction. II. The elastic range. Proceedings of the Royal Society of London. Series A 229, 198–220.

Whittaker, E.T., Watson, G.N., 2002. A Course of Modern Analysis. Cambridge University Press, Cambridge – New York – Melbourne – Madrid – Cape Town.

Zhuravlev, V.P., 1998. The model of dry friction in the problem of the rolling of rigid bodies. Journal of Applied Mathematics and Mechanics 62 (5), 705–710.

Zhuravlev, V.P., 2003. Friction laws in the case of combination of slip and spin. Mechanics of Solids 38 (4), 52–58.